Kaunas University of Technology

Faculty of mathematics and natural sciences

Phantom-Based Dosimetric Evaluation of Image-Guided Radiotherapy procedures

Master's Final Degree Project

Lamiaa Abdelrazik

Project author

Assoc. Prof. Jurgita Laurikaitienė

Supervisor

Kaunas, 2021

Kaunas University of Technology

Faculty of mathematics and natural sciences

Phantom-Based Dosimetric Evaluation of Image-Guided Radiotherapy procedures

Master's Final Degree Project

Medical physics (code 6213GX001)

Lamiaa Abdelrazik

Project author

Assoc. Prof. Jurgita Laurikaitienė

Supervisor

Lecturer Marius kaminskas

Reviewer

Kaunas, 2021

Kaunas University of Technology

Faculty of Mathematics and Natural Sciences

Lamiaa Abdelrazik

Phantom-Based Dosimetric Evaluation of Image-Guided Radiotherapy procedures

Declaration of Academic Integrity

I confirm the following:

1. I have prepared the final degree project independently and honestly without any violations of the copyrights or other rights of others, following the provisions of the Law on Copyrights and Related Rights of the Republic of Lithuania, the Regulations on the Management and Transfer of Intellectual Property of Kaunas University of Technology (hereinafter – University) and the ethical requirements stipulated by the Code of Academic Ethics of the University;

2. All the data and research results provided in the final degree project are correct and obtained legally; none of the parts of this project are plagiarised from any printed or electronic sources; all the quotations and references provided in the text of the final degree project are indicated in the list of references;

3. I have not paid anyone any monetary funds for the final degree project or the parts thereof unless required by the law;

4. I understand that in the case of any discovery of the fact of dishonesty or violation of any rights of others, the academic penalties will be imposed on me under the procedure applied at the University; I will be expelled from the University and my final degree project can be submitted to the Office of the Ombudsperson for Academic Ethics and Procedures in the examination of a possible violation of academic ethics.

Lamiaa Abdelrazik

Confirmed electronically

Abdelrazik Lamiaa. Phantom-Based Dosimetric Evaluation of Image-Guided Radiotherapy procedures. Master's Final Degree Project/supervisor Assoc. Prof. Jurgita Laurikaitienė; Faculty of Mathematics and Natural Sciences, Kaunas University of Technology.

Study field and area (study field group): Health Sciences, Medical Technologies (G09).

Keywords: IGRT, Halcyon, CBCT, IQ, Phantom, HU, Uniformity, Noise, LCV.

Kaunas, 2021. 70.

Summary

Image-guided radiotherapy (IGRT) has been regarded as the state-of-the-art technology for most sites. The ultimate reason for using more sophisticated and expensive technology is the improvement of patients' health. IGRT is used to treat tumors in areas of the body that are prone to movement. While IGRT provides more accurate treatment delivery, it is not without its challenges.

Therefore, the main advantages and disadvantages of different modalities of image-guided radiotherapy have been analyzed.

A new linear accelerator *Halcyon* with an integrated Image-guided Radiotherapy system has been installed recently in the Hospital of Lithuanian University of Health Sciences Kaunas Clinics, Oncology Hospital. The patient positioning before the treatment usually starts with accurate visualization of regions of interest (ROIs) within the patient, using image quality assessment (IQA) for KV/MV CBCT. Quality control (QC) is a critical step using the image-guided system for the patient positioning regarding internal organs visualization. Due to this reason Hounsfield units (HU) accuracy, HU uniformity, signal to noise ratio (SNR), a contrast to noise ratio (CNR), low contrast variability, slice thickness, and geometric scaling have been evaluated by using commercially available phantoms (*QUART and Gammex*) that contain multiple inserts tailored to test various aspects of image quality, using treatment planning system (*Eclipse*), and software (*RadiAnt)* and *(ImageJ)*. Each image quality parameter shows consistent imaging for the normalized mean and standard deviations. A conclusion can be stated that the KV CBCT image-guided system performance is accurate to perform IGRT and can be used clinically, but it is recommended to perform quality control tests due to prepared protocol monthly.

Lamiaa Abdelrazik. Vaizdais valdomos spindulinės terapijos procedūrų dozimetrinis įvertinimas, paremtas matavimais su fantomu / vadovė doc. dr. Jurgita Laurikaitienė; Kauno technologijos universitetas, Matematikos ir gamtos mokslų fakultetas.

Studijų kryptis ir sritis (studijų krypčių grupė): Sveikatos mokslai, Medicinos technologijos (G09).

Reikšminiai žodžiai: IGRT, Halcyon, CBCT, IQ, Phantom, HU, vienodumas, triukšmas, LCV.

Kaunas, 2021. 70 psl.

Santrauka

Vaizdais valdoma radioterapija (*angl.* Image-guided radiotherapy – IGRT) tai galimybė užtikrinti gydymo tikslumą radioterapijoje. Taigi naujų technologijų naudojimas yra glaudžiai susijęs ir su pacientų sveikatos gerinimu. IGRT yra naudojama vizualizacijai bei paciento pozicionavimo tikslumo užtikrinimui, ypatingai tais atvejais, kai navikas turi galimybę judėti anatomiškai (plaučių navikai, prostata ir pan.). Nors IGRT, tai galimybė užtikrinti apšvitos procedūros tikslumą, tačiau ši technologija turi ir savų iššūkių.

Taigi šiame tiriamajame darbe buvo išanalizuoti pagrindiniai privalumai ir trūkumai skirtingų vaizdinimo technologijų.

Neseniai Lietuvos sveikatos mokslų universiteto ligoninės Kauno klinikų filiale Onkologijos ligoninėje buvo sumontuotas naujas linijinis greitintuvas „Halcyon“ su integruota vaizdais valdoma radioterapijos sistema (IGRT). Todėl prieš pradedant apšvitos procedūrą atliekamas paciento pozicionavimas vizualizuojant dominančias sritis, naudojant skirtingus vizualizacijos rėžimus KV/MV (kūginio pluošto kompiuterinė tomografija (*angl.* cone beam computed tomography –CBCT). Kokybės užtikrinimas yra labai svarbus ir atsakingas žingsnis, naudojant integruotą vaizdinimo sistemą paciento pozicionavimui. Dėl šios priežasties Haunsfildo vienetų (HU) tikslumas, HU vienodumas, signalo ir triukšmo santykis (SNR), kontrasto ir triukšmo santykis (CNR), „pjūvio“ storis bei geometrinis fantomo matmenų vertinimas buvo atliktas naudojant komercinius fantomus („QUART“ ir „Gammex“), kuriuose yra skirtingų medžiagų intarpai, naudojami įvairiems vaizdo kokybės testavimams. Gautų rezultatų vertinimas buvo atliktas naudojant gydymo planavimo sistemą („Eclipse“), programinę įrangą („RadiAnt“) ir („ImageJ“). Išanalizavus gautus rezultatus nustatyta, kad KV CBCT vaizdais valdomos sistemos veikimas yra tikslus ir gali būti sėkmingai naudojama klinikinėje praktikoje, tačiau rekomenduojama atlikti kokybės užtikrinimo testus, pagal paruoštą protokolą.

Table of Contents

List of figures

List of tables

List of abbreviations and terms

Abbreviations:

IGRT – Image-guided radiotherapy

CBCT – Cone-beam computed tomography

CT – Computed Tomography

AAPM – American Association of Physicists in Medicine

IQ – image quality

KV – kilovoltage

MV – megavoltage

PTVs – planned target volumes

OARs – organs at risk organs

CTV – clinical target volume

HNC – head and neck cancer

LC –Lung Cancer

BC – Breast Cancer

GC – Gastrointestinal Cancer

PC – Prostate cancer

RTTs – Radiation therapy technologists

VMAT – volumetric modulated arc therapy

SRS – stereotactic radiosurgery

SAL – shrinking action level

NAL – No action level

MRI – magnetic resonance imaging

US –ultrasound

ACR – American College of Radiology

OBI –On-Board Imager

FPDs –Flat panel detector

EPIDs – Electronic portal imaging devices

FMs –fiducial markers

FOV –field of view

FBCT – Fan beam Computed tomography

SID – source imaging distance

FF – Full fan mode

HF – Half fan mode

CTOR – CT-on-rails

CNS – central nervous system

CNR – Contrast-to-Noise Ratio

QA – quality assurance

HU – Hounsfield unit

QC – quality control

IMRT – intensity-modulated radiation therapy

FFF – flattening filter-free

MLC – multi-leaf collimator

TP – treatment planning system

ROIs – regions of interest

UI – uniformity index

CNR – Contrast-to-Noise Ratio

LCV – low contrast visibility

SD – standard deviation

RSD – standard deviation ratio

FWHM – Full width of half maximum

Introduction

The cancer patient can be treated by two types of radiation therapy: external beam radiation therapy or internal source radiation therapy. Internal source radiation, then the source is" placed" inside the target is known as brachytherapy, while external beam radiation therapy (EBRT) is typically performed, then the source is outside the patient. Due to this reason, EBRT usually is followed by image-guided radiotherapy (IGRT).

Image-guided radiotherapy (IGRT) is a technique employing an imaging process during radiation therapy (RT) delivery, aiming to improve the accuracy of treatment. IGRT allows visualization of anatomical details and guiding any changes in tumor and position of the volume in real-time or near real-time. In another word, IGRT uses different imaging modalities for the patient positioning and target localization visualization accurately before and during treatment fraction. IGRT technologies spread rapidly over the last decade, especially in some cases such as lung, prostate, and gastrointestinal tract cancers.

Cone-beam computed tomography (CBCT) is In-Room CT-based image guidance technique that routinely is used for the patient setup verification and position adjustment to deliver treatment with high precision. The accuracy of the image-based procedure is a very *important* and r*elevant* step, which depends on the quality of the obtained images. Hence, the American Association of Physicists in Medicine (AAPM) and other professional organizations [1] strongly recommend periodic image quality (IQ) evaluation, but there has been no consensus on uniform acceptance for the CBCT image quality verification yet. The recommendation can be performed by physicists and IQ evaluation can be done by using a phantom specifically designed for these tests. IQ can be evaluated by using simple methods for image noise, and low- and high-contrast resolution measurements, but there are more quantitative and accurate methods to evaluate the CBCT image.

*This research project aim*s to perform phantom-based dosimetric analysis for image-guided radiotherapy.

The tasks:

1. To analyze the main advantages and disadvantages of different modalities of image-guided radiotherapy.
2. To perform and analyze phantom-based quality control measurements for newly implemented linear accelerator *Halcyon*.
3. To adapt the protocol of quality control for use in a clinical practice.

Phantom-based dosimetric analysis was performed in a Hospital of Lithuanian University of Health Sciences Kaunas Clinics, Oncology Hospital, radiotherapy department.

1. Literature Review

1.1. Definition and Rationale of Image-Guided Radiotherapy

The goal of treatment in radiotherapy is to deliver the dose to the planned target volumes (PTVs) of the patient and minimize the dose outside the target, decreasing the risk of damage to healthy tissues or organs at risk. The process of dose delivery must be done as precisely and accurately as possible.

It is known that accuracy depends on radiation treatment planning and delivery technique, which allow much more conformal distribution of the dose, sharper dose gradients, higher doses per fraction (dose escalation), and reduction of toxicity. Therefore, the accuracy of treatment delivery is more crucial because it is needed to control possible geometric uncertainties and enhance target delineation/ contouring for the planning and target localization before or/and during the treatment procedure.

Special attention is paid to the treatment of moving targets/ cancers, for example, lungs and breast, which are affected by the breathing process, while the prostate moves according to pelvic organs movement, for example, due to rectal and bladder fullness or/and emptiness may affect the quality of the treatment procedure. Also, it is known, that during the treatment course, volumetric changes can occur for the target and organs at risk organs (OARs), due to irradiation or/ and hormonal therapy. Therefore, there are many factors of uncertainties in radiotherapy workflow, which can influence the accuracy of the treatment [2]. Factors of uncertainties and errors that occurred during radiotherapy planning and delivery processes are classified as treatment-related and tumor-related factors. It may lead to uncertainty for the delineation of the target volume, the variation of organ positional, and set-up errors [3]. Setup errors can be defined as any differences between intended and actual treatment positions during radiotherapy. Setup errors are related to patient positioning or rotation, weight loss, contour deformation due to tumor shrinkage, skin marker shift, involuntary motion, and tensing of muscles. Setup errors are classified as systematic errors and random errors. The systematic errors are treatment preparation errors, these errors influence all the fractions. For example, organ motions between the planning scans and the start of treatment. The cause of these errors can be errors in a unit set-up, faulty instruments, or modeling or error in incorrect usage of the equipment. Systematic errors may cause overdose/under-dose of the target volume or cause changes of the dose distribution in comparison with a planned clinical target volume (CTV). These errors can be corrected before the treatment. Random errors are treatment execution errors, affecting each fraction separately and being unpredictable. Random errors may insignificantly affect the dose distribution around CTV [4]. Organs' motion and deformation may affect volume changes, bladder and/ or rectal filling, intra-abdominal pressure, bowel gas, respiration, cardiac motion, peristalsis. It can be corrected daily within the treatment. There are also two subcategories' classifications, which include so-called intrafraction motions and interfraction motions. Intrafraction motions mainly occur within the treatment fraction due to organ motion, while interfraction motions mainly occur from fraction to fraction due to setup irreproducibility such as positioning errors and anatomy changes [5,6].

To avoid these problems and minimize the factors of uncertainties, improving the treatment accuracy, an additional technique should be implemented in the treatment room which employs an imaging process for guiding any changes in the treatment area (target or/ and OARs location, shape, and size) before and during each treatment fraction. This technique is known as Image-guided radiation therapy (IGRT) and

can be defined simply as usage of imaging modalities (such as X-ray, CT scan, MRI, or ultrasound…. etc.), which generate images (for bony or/ and soft tissues before or/ and during the treatment procedure, comparing them with the reference images taken during simulation) throughout the entire process of radiotherapy. After mentioned comparison, the practitioner decides for repositioning the patient and/ or adjustment of the radiation beams. So could be delivered radiation dose to the tumor more precisely and minimized radiation harm for the healthy surrounding tissues. The image-guidance process means and additional time to each radiation therapy session, but this is beneficial and ensures the quality of the treatment.

Image-guided radiation therapy (IGRT) leads to reduce geometrical uncertainties, evaluating patient geometry during the treatment, and either altering the patient position or adapting the treatment plan according to anatomical changes, which occur during a course of radiotherapy.

Several studies have been done to confirm the benefit of IGRT usage with different treatment modalities. It could be used with intensity-modulated radiation therapy (IMRT), 3-D conventional radiation therapy (3D-CRT), heavy particle therapy (proton/neutron), or even stereotactic radiosurgery, or stereotactic body radiotherapy (SBRT) [7-10]. However, the IGRT techniques advancement have shifted to use adaptive radiation therapy (ART), where image guidance is used in conjunction with image registration and replanning (creation of new treatment plan (if necessary)), which is adapted to the current patient anatomy if it is sufficiently different than the initial plan.

IGRT is used to visualize tumors in areas of the body, which are prone to movement, as well as a tumor located close to critical organs and tissues. Types of cancer treated using IGRT technologies for visualization are head and neck cancer (HNC), Lung Cancer (LC), Breast Cancer (BC), Gastrointestinal Cancer (GC) (such as stomach and gastrointestinal stromal tumors), and Prostate cancer (PC) [10].

The benefits and advantages of IGRT include increased accuracy of radiation treatment, improved implementation definition, localization and monitoring of target position and movements before and during treatment, allowed the possibility of higher, targeted radiation dosage and improved tumor control, at the same time reducing the radiation exposure for the surrounding healthy tissues, OARs and reduce overall treatment toxicity. While the disadvantages of IGRT are there is no single technology or strategy of every clinical implementation scenario and increase in precision of delivery of the dose also increases the importance of tumor detection and delineation errors [11].

1.2.The main problems and challenges

Image-guided radiotherapy (IGRT) has been considered a state-of-the-art technology for most of the sites. Even if IGRT provides more accurate treatment delivery, it does not mean, that it does not have any challenges. Some factors should be taken into consideration to assess the potential of benefits, before introducing any sophisticated modern and costly technology.

1.2.1. Clinical outcomes

Clinical Trials are considered the standard of evidence-based medicine. In most cases, IGRT has achieved good results in accuracy and precision (i.e. the reduction of margins) [12], but in other cases, IGRT has

led the user to some sort of disappointment [13]. Schwarz et al. [12] evaluated the effect of image-guided radiotherapy (IGRT) on the clinical target volume (CTV) dose and the organ at risk (OAR) versus non-image-guided radiotherapy (non-IGRT) during treatment of head-and-neck cancer (HNC) patients. They found that both techniques had the same impact on the CTV coverage, but IGRT has an advantage where it was able to spare the spinal cord by reducing the margin, while the non-IGRT approach has added additional margin which leads to an increase in the spinal cord dose more than the original plan [12].

Pushpa and Umesh [13] found that the imaging and biology-related uncertainties are not corrected by IGRT for gynecological malignancies, therefore, they overlooked the promise of IGRT to be able to reduce PTV margins. They suggested decisions regarding re-planning under strict IGRT protocol including serial documentation of target and organs at risk (OARs) deformation and their doses [13].

However, the clinical outcomes have not been documented well since some of the late toxicities may be observed years after giving radiation. Some studies have documented significant toxicity reductions pre-and-post-IGRT implementation in some sites such as prostate and head and neck cancer [14,15]. In many other disease sites, there is a good correlation between toxicity and the irradiated volume, where there are clinically significant toxicity reductions can be expected due to the usage of IGRT.

Also, Kupelian et al. [16] paid attention to the low rates of toxicity, independence of results from the rectal volume at the time of CT planning, where the daily IG can offset the systematic errors introduced at the time of the simulation.

The radiation oncologist needs to prescribe the type of IGRT and frequency of image acquisition, balance the clinical evidence of the benefits of IGRT against the expected dose to the patient, as advised by the medical physicist.

1.2.2. Cost outcomes - Cost /benefit ratio of new technology

The idea behind IGRT is to expose the patient to two types of doses: therapeutic doses that are used for the treatment of cancerous tissues and imaging doses that are used for tumor localization. Therefore, it is mandatory to justify the medical exposure by weighing the diagnostic or therapeutic benefits [17]. The benefits of IGRT implementation need to be balanced against other factors such as 1) costs, 2) added time, and 3) complexity of treatment.

Most clinical scenarios showed that the benefits outweigh the costs. The balance between benefit and cost should be maintained and improved even with improving image quality, reducing the imaging dose, and increasing the speed of the imaging process [18].

The ratio of both doses (imaging dose to therapeutic dose) depends on many factors such as the type of used imaging modality, the setting of procedures and its frequency, the prescribed dose, the size, and the age of the patient. Zhou. et al. [19] evaluated the cumulative imaging doses, the associated risk, and the cost related to the various radiological imaging procedures for IGRT. They reported that the average ratio of the imaging dose to the therapeutic dose was 0.65% and about 0.2% of patients had a ratio greater than 5%. Therefore, they recommended that the benefit/risk of image guidance should be evaluated carefully [19].

1.2.3. Potential risk

IGRT, like any form of radiation therapy, may cause side effects. Some studies showed that there is a positive correlation between ionizing radiation and cancer risk [20, 21] where the patient who undergoes the frequent imaging receives considerable doses to radiosensitive organs and may lead to higher radiogenic cancer risk to the patients, especially children. As a function of patient size, pediatric patients could receive much higher doses than adults. Increased secondary cancer risks and disease were strongly related to higher imaging doses and patient size.

1.2.4. Additional Training

Before IGRT implementation, it is important to train the medical physicists before the arrival of the equipment to be able to carry out acceptance testing and commissioning. Also, training and education in medical imaging are mandatory for the physicist who is specializing in radiotherapy [18].

Radiation therapy technologists (RTTs) who are including Radiation oncologists and radiation therapists will be decision-makers for patient setup adjustments, therefore, additional relevant education, training, and experience are required during, or before, the commissioning phase. They should achieve a specified set of learning outcomes [18].

1.3. Correction Strategies/ protocols

Analysis of acquired images is one of the steps to ensure the correct patient's positioning before the treatment procedure. Due to this reason could be used various categories of IGRT correction strategies in clinical practice. Two main protocols: offline and online are used in daily practice. Both have their own merits and can be selected in a specific clinical usage. The decision of selection of the protocol depends on the site being treated and departmental resources, including the need to balance the accuracy of treatment with expertise and workload. Magnitude and variability of intra-and interfraction motion. The most used strategy is online measurement and adjustment of position. For online adjustment, decisions should be made about the tolerance for a correctable action, considering both the accuracy with which measurement and correction can be realistically applied and the sensitivity of plan objectives to these actions.

1.3.1. Online correction protocol

On-line correction is defined as the image acquisition, image verification, and (if needed) correction application before each treatment session (i.e., before the day's treatment). The purpose of using an online strategy is to control and reduce systematic and random errors. This strategy is simple, clear, and by using this strategy, both errors can be corrected effectively but it may increase the time of treatment session but there is no need for additional effort for planning (However, in each treatment session, additional procedures for image acquisition, registration, patient positioning correction and verification need to be added). On-line strategy requires a high level of integration of both hardware and software and fast speed. The frequency of online imaging may be determined by the treatment site and the expected magnitude of the error. For example, daily imaging can be applied for the sites that may be expected to occur a large daily shift (such as thorax, abdomen, and pelvis) or slight shift but with changes in the dose distribution within adjacent critical structures (such as intracranial tumor near optic structures) [20].

The maximum errors were observed in the thorax followed closely by the abdomen and pelvis and the minimum errors were observed in the head and neck region [21]. The volumetric modulated arc therapy (VMAT) and stereotactic radiosurgery (SRS) have the probability to translate slight shifts into a considerable change in dose distribution, therefore daily online verification is required. The online IG uses population-based margins.

1.3.2. Offline correction protocol

The off-line correction strategy is defined as the image acquisition before treatment and makes a match to a reference image later, off-line (i.e., without the patient on the couch). The purpose of using an off-line strategy is to determine and reduce the individual systematic setup error or we can say to correct the mean error in positioning, without imaging at each treatment fraction (without affecting the time of each treatment fraction).

In general, the online IG uses population-based margins, and the offline IG uses patient-specific margins. The population-based systematic error is calculated as the standard deviation of the systematic errors of all patients within the treated population.

The purpose of the strategy is to reduce the magnitude of the individual patient systematic setup error and it can help to define and calculate the population standard error for that treatment in that institution by combining with setup data of other patients treated under the same protocol [22]. Offline correction protocols that are used widely include both protocols No action level (NAL) and shrinking action level (SAL) protocols. In the no-action level protocol, the systematic error is assessed by taking images during the first few fractions, and a setup correction is then generated and can be applied to the remaining fractions. After the mean error initial assessment and to ensure that the mean setup position has not changed, setup images are taken weekly.

In this protocol, the deviations of previous fractions are taken into consideration and analyzed, and this in turn aids to determine the set-up of the following fractions. Off-line protocols are effective in the correction of systematic effects, which, if uncorrected, have been verified to cause a shift in the cumulative dose distribution. Off-line correction protocols are therefore most appropriate when the ratio of random to systematic deviation is small.

1.4. The technology of image-guided radiotherapy

Any IGRT system consists of four main stages:

1. Image acquisition system. The image acquisition system (computed tomography (CT), magnetic resonance imaging (MRI), ultrasound (US), x-ray……)) is used together with radiation delivery units (Linear accelerator in case of x-ray/photon beam or cyclotron/synchrotron in case of charged particles beam), to image the target, bony, and/ or soft-tissue anatomy immediately before or during the treatment. There are other methods, which depend on using markers placed on the surface of the patient's body or implanted within the patient's body.
2. Set of reference images, taken during simulation, for comparison.
3. Specialized computer software for the comparison match between reference images and CT planning.
4. Protocol to define the correction method. The correction method could be online (i.e. before turning on the radiation beam) or offline between fractions.

The IGRT systems have been generally classified according to the used modality into radiation-based and non-radiation-based systems as reported by IAEA, Human Health Reports No. 16 [18]. Radiation-based systems are known, as Electronic Portal Imaging Device, CT-based image guidance, and non-radiation-based systems – Ultrasound Guidance, Electromagnetic Transponders, MR Guidance, Optical Systems. The non-radiation-based systems have superior advantages on the radiation-based system, where the patients are not exposed to an extra radiation dose, for example, providing information for additional images used evaluating intra-fraction motion.

Another approach was reported by the American College of Radiology [ACR] and the American Association of Physicists in Medicine [AAPM] [1] where the classification was done according to the projection types (Number of dimensions of image acquisition): 2-D (planar or surface) approaches (e.g., MV portal imaging and KV imaging) and 3-D volumetric approaches (e.g., cone-beam CT and helical CT) [1]. The most important point of difference between planar and volumetric approaches is the ability directly to visualize the soft tissues, where the planar imaging uses a surrogate to define the organ position, while the 3D volumetric approaches can visualize the soft tissues directly, with the ability to adapt the treatment plans according to any changes for the target and OARs before each treatment fraction over the total treatment course. The acquisition process of 3D images is slower than the acquisition of 2D images, but its interpretation is easier, faster, and more accurate than planar imaging, and therefore, 3D volumetric imaging has become the standard of image guidance in current radiotherapy (RT).

There is another classification related to hardware, which was reported by Chen et al. [23] where was classified into three categories. The first one is Gantry mounted (On-Board Imager, OBI), where a gantry mounted Kilovoltage kV imaging system on a linear accelerator (orthogonal to the therapy MV x-ray beam). The flat-panel imager and x-ray source are mounted on retractable arms. Kilovoltage x-ray imaging offers images with near-diagnostic quality. With either kV or MV imaging, determination of the correction to the position of the patient uses orthogonal image pairs that are matched to the reference image. The second category of kV imaging is ceiling/floor-mounted systems (Room Mounted). These systems provide an oblique orthogonal image pair for 3D imaging at a wide range of angles of the

treatment couch and consist of two kV X-ray tubes, two Flat panel detector FPDs, two IR cameras, one video camera, and an IR marker array. The third category is Rail-track/Wheeled systems [23].

At present, in clinical use, there are a variety of commercial IGRT technologies available to apply. Depending on the used clinical scenarios such as the tumor site, the expected errors, and the purpose of the application (patient positioning, target localization, or tumor tracking in real-time mode), the IGRT system can be chosen. It means, that the systems, which are used to correct only interfraction displacements (set-up differences) can be different from the systems, which are used for intrafraction movements. The decision should be taken by the radiation oncologist. Each system has its advantages and limitations. In some cases, MV portal imaging is enough for localization and achieving the required accuracy on the order of centimeters (cm), for the other cases, related to critical structure, daily kV or CBCT is required to minimize setup uncertainties to the order of millimeters (mm). In cases of hypofractionated treatment (SBRT or SRS), a real-time tracking system might be an optimal solution for tracking intra-fractional motion [24]. For the large facilities, there is a possibility to have integration of multiple IGRT systems into one single room, for instance, integration of 3D ultrasound to Cone-beam CT (CBCT) for prostate treatments [25]. More IGRT technologies are implemented better geometric precision it means, which leads to improving the quality of patient care [24].

This section presents a rough overview of these technologies, describes some applications, and shows some of their advantages and disadvantages.

1.4.1. Electronic Portal Imaging Devices (EPID)

Electronic portal imaging devices (EPIDs) (Fig. 1) are an alternative to film dosimetry for treatment verification and are used to measure the intensity of the X-ray that is transmitted from a radiation port through a patient during a treatment session. The Flat-Panel detector is a matrix of detectors with amorphous silicon photodiodes. The detected radiation signal is converted into a two-dimensional (2D) digital radiographic image electronically. EPID can be used for setup error reduction, treatment verification, and quality assurance. There are two different systems, that is, KV X-rays and MV X-rays for imaging. In the case of the MV system, the photons interact with patients mainly through Compton scattering (atomic number independent). Therefore, the image contrast in the KV system is superior but there is lesser distortion in MV images in the case of metallic implants such as dental, hip prosthesis. for KV systems, the average dose per image is 1–3 mGy while it is 30–70 mGy for MV systems [26].

Fig. 1. Electronic Portal Imaging (EPID) [27]

The information of the image (from both: Megavoltage x-ray electronic portal imaging (EPI) and Kilovoltage x-ray portal imaging) provides bony landmarks as an aligning surrogate, but it has lacks soft-tissue contrast. Therefore, Soft tissue imaging can be achieved by implanting a surrogate (i.e., fiducial markers (FMs)) to track mobile tumors [26]. The most used fiducial markers for the prostate are small gold seeds. Three FMs can be used as a surrogate for the positioning of the prostate. Due to its inert, radioopaque nature of gold, it is considered an ideal substance for implantation. It is a non-invasive process but could track intra-fraction motion.

The advantage of portal imaging techniques is that using the treatment beam for imaging, therefore, there is no need for an extra dose however, some information on internal anatomy can be provided.

The disadvantages of portal imaging techniques are, it is a 2D technique and cannot provide a 3D definition of anatomy information. The verification is not done in real-time, and it could lead to adding a large margin to compensate for the set-up error and inter-and intra-fractional motion. Besides, using higher energy x-ray may affect the image quality.

1.4.2. In-Room CT-based image guidance

In-Room CT-based image guidance is a type of IGRT technology that depends on using the diagnostic Computed Tomography (CT) in the treatment room. This technique has many advantages over the planer imaging techniques where the diagnostic CT provides volumetric anatomic information (3D) and the better visibility of soft tissue. These both factors are useful for accurate target localization and patient positioning verification [28]. It is also useful for dose computation that can be used to track the delivered dose distribution. Frequent comparisons of the delivered dose to the planned dose distribution enable one to make setup corrections or adjust the treatment plan to minimize the variations between the planned

and the actual delivered dose, which is known as the image-guided adaptive radiation therapy (IG-ART) [29,30].

There are two methods of the CT image acquisition process for the verification of patient setup where there is only one couch for the patient. The first method with the treatment table of the actual treatment machine, where the patient on the treatment couch must be moved between the scanner and the treatment unit, or the second method with the CT scanner (and/or the treatment unit) moved to/from the patient. This introduces different sources of error: the time taken to move the patient or the equipment, the tolerance of the motion of the system, the patient reacting to being moved, and the inherent separation of imaging and treatment isocentre.

In-Room CT-based image guidance can be classified into two main categories. The first category is according to the beam quality (Megavoltage MV or Kilovoltage kV), the second category is according to beam collimation (Fan-beam or Cone-beam).

Held M, et. al, [31] paid attention to the reason for the different appearance of kV and MV images (Fig.2) that results from the higher proportion of Compton scattering and high-energy electrons in MV x-ray beams relative to kV x-rays (photon attenuation is independent of the atomic number Z). Therefore, the kV-imaging technique is superior to MV-imaging, due to image quality, low imaging dose, and enhanced soft-tissue image contrast due to the predominant photoelectric interactions at low energies that are proportional to Z^3. Also, they noted the shades of Gray-level around bony anatomy are brighter in kV CBCT images.

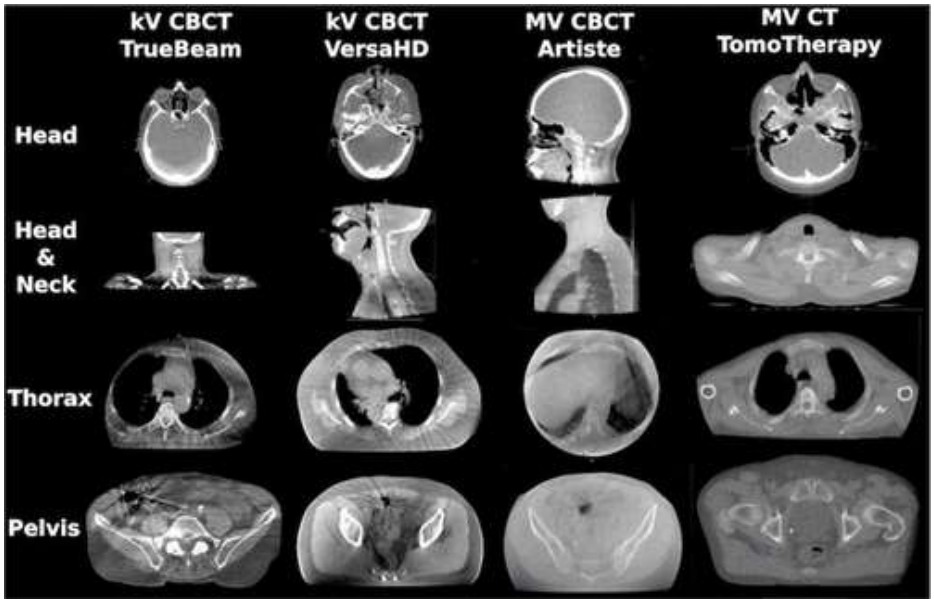

Fig. 2. Patient CT images of different treatment sites [31]

As has been mentioned above, the image quality of the MV beam is inferior compared to the kV beam, but due to accurate electron density estimation, the MV beam has lesser distortion and can reduce metal artifacts, which is useful for patients with metallic implants such as dental or hip prosthesis. (Fig. 3) [32].

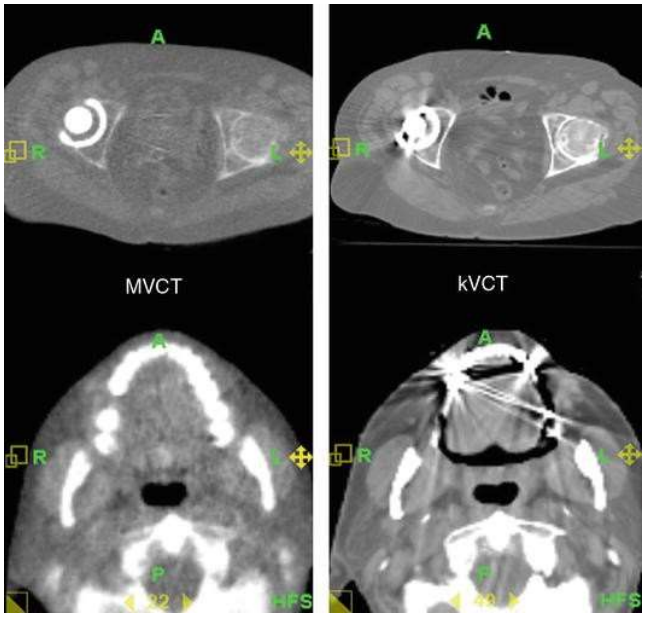

Fig. 3. The impact of implanted metal on MVCT and kV CT images [32]

This section describes the classification In-Room CT-based image guidance according to beam collimation.

The first type is the fan-beam systems that use a linear detector array in an arc to detect the helix/spiral beam (Fig. 4, Fig. 5. A) which is emitted from a rotating fan-beam X-ray source. This technique produces a single slice image per scan. The radiation source turns around the patient continuously where the target volume is irradiated slice by slice leads to receiving a higher dose to different sub-volumes (for instance, the red dot in Fig. 5. D). [33]. This system can be integrated with a linear accelerator in the treatment room for both treatment and imaging or can exist as a peripheral CT gantry. The advantages of fan-beam CT include greater soft tissue definition and greater bone resolution.

The second type is the cone-beam system. Cone-beam CT system (CBCT) is a recent development that uses a cone-beam emitted from an X-ray source in the shape of a cone (Fig. 4 and Fig.5. B) where it can cover a large volume with one single full rotation (360 degrees about the patient) (Fig.5. C). CBCT acquires projections onto the 2D detector. All slices are reconstructed from one signal rotation of the gantry. A filtered back-projection algorithm is used to reconstruct the 2D projected image into 3D volumetric images of the target volume. The speed of image acquisition depends on the scan time which equals the time of one gantry rotation, gantry speed (~1min/rotation). Then, the volumetric images are compared with the planning CT images, and a decision is made for patient positioning to determine the set-up error or tumor motion. CBCT imaging can visualize the location of the exact tumor just before patient treatment on a linear accelerator. The efficacy of CBCT-IGRT is expected to increase further through better reconstruction algorithms [34-36].

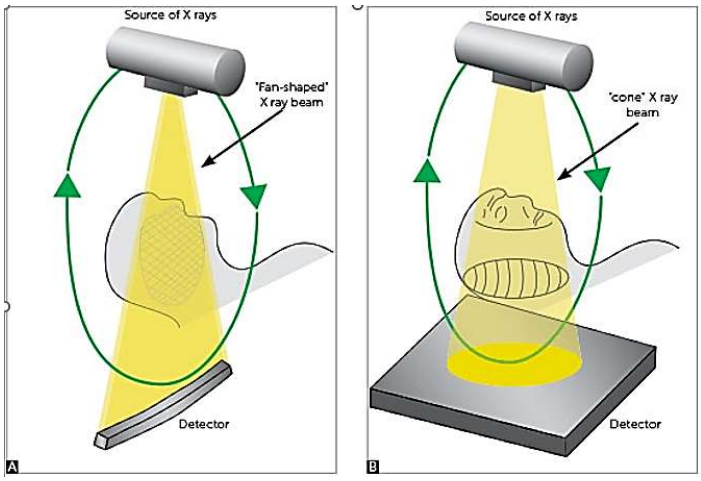

Fig. 4. Projection of X-ray A) Fan Beam B) Cone Beam [39]

The three main clinical roles of CBCT are verifying patient positioning, tumor localization, and tumor change tracking during treatment. The Advantages of CBCT include lower radiation dosage, fewer artifacts with metallic objects, lower cost, Possibility to operate by non-radiologists [37]. CBCT provides a detailed snapshot of the anatomy before treatment, provides high spatial resolution for daily positioning; but due to the length of image acquisition, this technique is not a good solution to be used for intrafraction motion management. The usage of CBCT as IGRT helps reduce healthy tissue exposure, although the dose delivered to the patients is higher than the dose delivered by fan-beam CT [38].

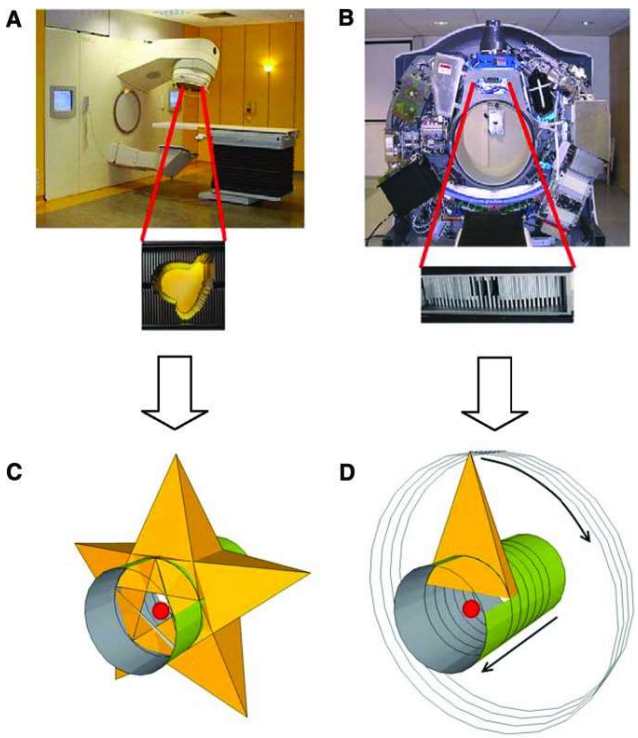

Fig. 5. Fan-beam and cone-beam CT imaging techniques (A): cone-beam multileaf collimator in linear accelerator with (B): Binary fan-beam multileaf collimator of Helical tomotherapy. (C): irradiation of the target volume by Cone-beam continuously. (D): irradiation of the target volume by the fan-beam slice by slice [33]

AS the CBCT machine operates with lower energy than diagnostic machines to reduce exposure dose, this leads to lower signal-to-noise in CBCT than in fan-beam CT. The Cone beam (CBCT) images include a big amount of scattering when compared to fan-beam FBCT. Scatter is a result of the larger detector area / larger field of view (FOV) of cone-beam geometry. This leads to photons' deviation from their path and increases the incident intensity causing artifacts. This may result in streaking and lower soft-tissue tissue contrast [40, 38]. Due to the above reasons, imaging on CBCT is of poorer quality than diagnostic CT. Phantom studies have shown that key imaging characteristics such as low-contrast visibility, spatial resolution, uniformity, and image noise are all inferior for CBCT compared to diagnostic CT [40]. Lechuga, et al. have been compared between Cone-Beam CT (CBCT) and Fan-Beam CT (FBCT). the results revealed that the CBCT has a superior spatial resolution to that of the fan-beam, while the fan-beam has a greater ability to produce clear and anatomically correct images with better soft tissue differentiation. The results indicate that FBCT produces superior images to that of cone-beam CT systems while providing a less dose to the patient (Fig. 6) [42].

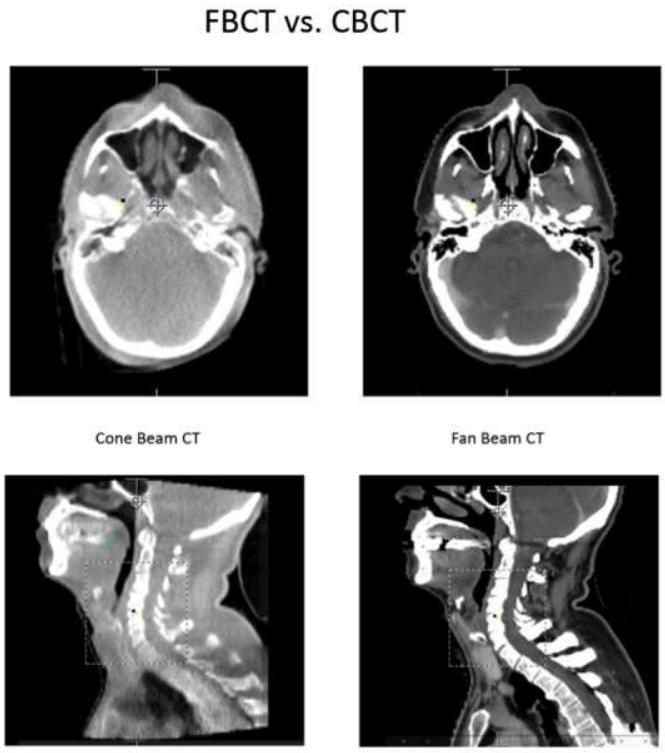

Fig. 6. Cone-beam CT image (left) vs. fan-beam CT image (right) of head and neck IGRT case in axial and sagittal orientation [42]

There are two different modes of acquisition geometries, Full fan mode (FF) or half fan mode (HF) (Fig. 7). The selection of modes is dependent on the size of the treatment site. For instance, in the case of skull imaging or Head and neck imaging, the full fan mode is used to image the entire patient volume-of-interest (VOI) in each projection over a ~180° arc, and the maximum field-of-view FoV of 24 cm is possible at the source imaging distance SID= 150 cm. In the case of the thorax and pelvis, a larger field-of-view (FoV) is required. Therefore, the cone beam and detector are offset laterally to increase the FoV (Half fan mode is used) and it is required a longer arc ~360°. The maximum FoV of 45 cm is possible at

source imaging distance SID= 150 cm. If the FoV is larger than 24 cm, the CBCT acquisition is automatically switched to Half fan mode.

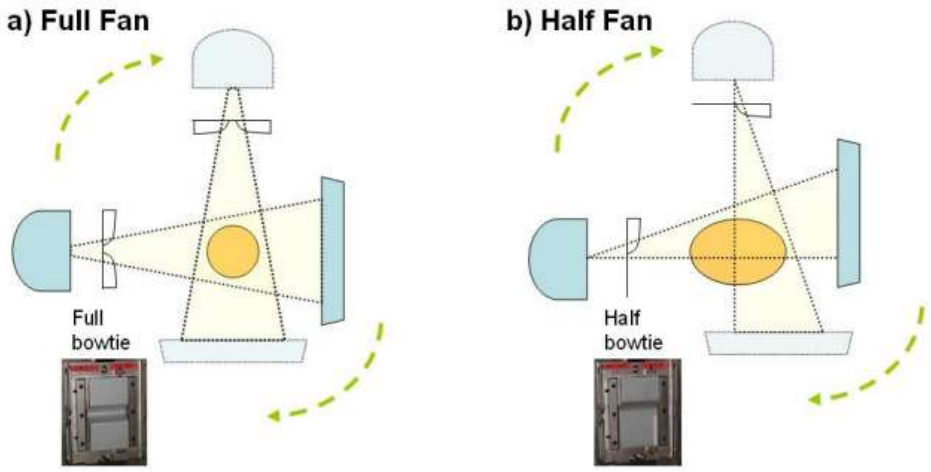

Fig. 7. Acquisition geometries modes: a) Full fan mode (FF) b) Half fan mode (HF) [43]

According to the above two classifications, beam quality and collimation classifications, there are four main types of in-room CT-based image guidance technologies are available:

1.4.2.1. Megavoltage Fan Beam CT (MV FBCT):

Hi-Art TomoTherapy is an example of integrated helical fan-beam megavoltage CT (Fig. 8) The tomotherapy system, consists of Linac (6 MV) which is mounted on Ct type gantry ring to rotate the linac around a patient. During treatment, the patient on the couch is inserted through the gantry bore to deliver the radiation dose to the target volume in helical geometry. The system is designed to acquire the image at any time before, during, or after treatment by using a xenon ionization chamber consisting of a 738-element array that rotates on the gantry opposite the linac.

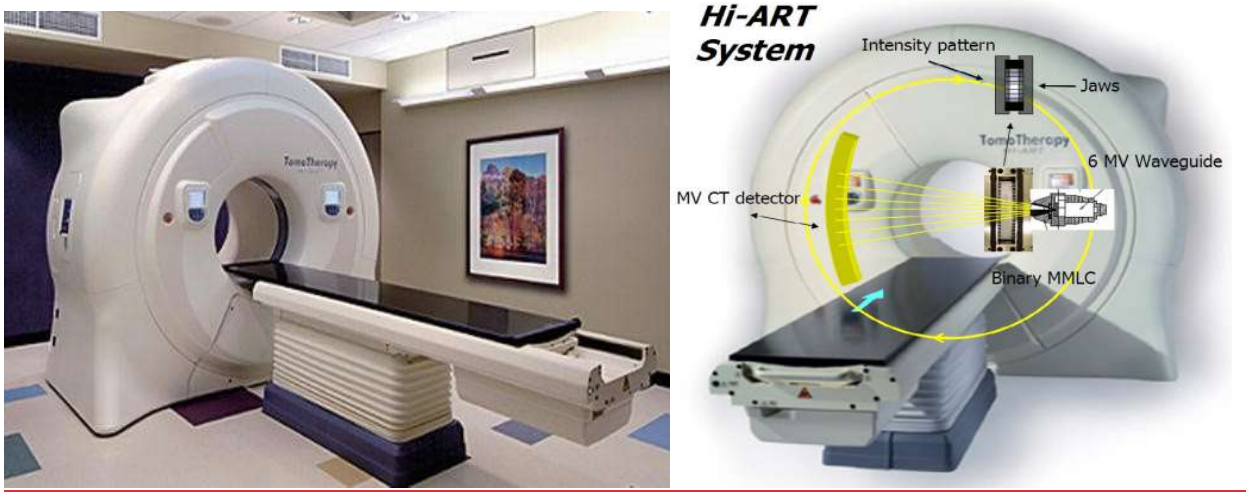

Fig. 8. Hi-Art helical tomotherapy CT-guided IMRT system [32, 44]

Megavoltage CT (MVCT) does not need for uses additional x-ray sources or detectors to make a scan because it uses the treatment beam to scan too. The limitations of MVCT in comparison with diagnostic energy CT arise from the lower quantum efficiency of a detector at the megavoltage energy and the lower intrinsic contrast between the various tissues. However, trade-offs may be made in terms of quantities such as the spatial resolution required, to limit the dose needed.

1.4.2.2. Megavoltage Cone Beam CT (MV CBCT)

For instance, Siemens Artiste or MVision® are examples of integrated megavoltage CBCT systems). The MV-CBCT system consists of a conventional EPID with an amorphous silicon flat-panel detector (FPD). In this case, the X-ray source is the treatment beam.

The advantage of megavoltage CBCT is that no additional equipment is required for producing the cone beam since beams come from the linear accelerator. Besides, MVCT systems use the detector panel that is already installed on the linac for use in electronic portal imaging.

1.4.2.3. Kilovoltage Fan Beam CT (kV FBCT):

CT-on-rails™ (CTOR) is an example of peripheral fan-beam KV CT which consists of a diagnostic CT gantry mounted in the treatment room, and linac-integrated kV imaging equipment, consisting of an X-ray source for imagining and a flat panel electronic imaging device (PEID) (Fig. 9) A concern of the CT-on-rails technology is that the movement of the patient couch between the treatment machine and the CT scanner may lead to undetectable setup errors [45].

Fig. 9. Siemen's CTVision consisting of a Primus linear accelerator and a modified SOMOTOM diagnostic CT scanner [46]

1.4.2.4. Kilovoltage Cone Beam CT (KV CBCT)

(For example, Varian On-Board Imager® (OBI®) (Fig. 10) or Elekta Synergy® XVI ® systems are examples of gantry-mounted kilovoltage CBCT systems)

The KV-CBCT system consists of a conventional X-ray tube which is mounted on a retractable arm (perpendicular) at 90º to the high-energy treatment beam. A large flat-panel detector (FPD) is mounted on a retractable arm opposite the X-ray tube [33].

The principal factor is the non-collimated geometry which results in increased scatter reaching the flat-panel detectors. CBCT images are subject to reducing signal-to-noise ratio (SNR), streaking and cupping artifacts, and reducing the contrast (especially for soft tissue). The gantry rotation speed is slow and also limits the CBCT image quality as image blur occurs from patient motion (internal and external motions) [38].

A study has been done by Morrow NV, et al. [49] to compare the image quality of kV CBCT (Synergy; Elekta) with different computed tomography modalities, such as megavolt CBCT (MVision; Siemens), megavolt FBCT(Tomotherapy), and kilovolt FBCT (CTVision, Siemens), where they assessed the image quality of kV FBCT as the highest image quality (IQ), followed by kV CBCT, MV FBCT then MV CBCT.

Chan et al. [49] have evaluated the imaging performance of four clinically CBCT/FBCT systems (Varian kV CBCT, Elekta kV CBCT, Siemens MV CBC, Tomotherapy MV FBCT) The results state that Elekta CBCT providing faster image reconstruction and low dose per scan for half-circle scan, Varian CBCT had lower image noise, and Tomotherapy FBCT had the best uniformity.

Fig. 10. Varian On-Board Imager (OBI) [47]

In conclusion, in-room CT-based guidance currently is the standard for image guidance. It is more suited for tumors in the brain, head and neck, lung, or breast. Due to motion blurring (CBCT) or motion distortion (CT), CT-based guidance is less so for abdominal organs [50].

The disadvantage of CT-based methods remains in the limited resolution of onboard imaging systems which creates a challenge in determining the precise location of the target, as well as the image acquisition time duration, prohibiting its use for intrafraction motion monitoring or correction [51].

1.4.3. Ultrasound (US)-based image guidance System

Numerous ultrasound (US) systems have been developed for soft-tissue verification in radiotherapy, with particular application to prostate localization. In this approach, conventional ultrasound systems are utilized in conjunction with an optical tracking system or robotic tracking system to allow ultrasound images of internal anatomy to be related to the treatment unit isocentre. The ultrasound systems are used in various applications in radiation therapy especially in the localization of prostate cancer treatment and breast cancer treatment.

The advantages of ultrasound Guidance systems are non-invasive, real-time tracking, providing a volumetric image with a high contrast of soft tissue, integrated easily within the RT process, reducing patient setup times, relatively low-cost, and free toxicity [51, 52]. Nevertheless, there are some concerns because the accuracy and precision of this system depend on a skilled operator. For localizing prostate There are some challenges such as (1) image quality is low; (2) an unfamiliar appearance of images, leads to larger inter-and intra-observer variability (the recommendation, in this case, is to use a large margin); and (3) the potential errors arising from anatomic distortions due to the probe pressure on the abdomen.

The BATCAM$^{@}$ and SonArray$^{@}$ Systems utilize US imaging only for patient setup have a hand-held US probe (2D for BATCAM and 3D for SonArray) with attached optical markers. These markers can be tracked by cameras mounted on the ceilings of both simulation and treatment rooms. Newer systems such as the Elekta Clarity$^{@}$ System employ 4D monitoring using a remotely operated ultrasound probe. It can use US imaging for both patient setup and real-time monitoring during radiotherapy [53]. The difference between this system and other systems is that the US probe is attached to a passive arm mounted on the couch and acquires 3D US images before and during, treatment. For patient setup, this system compares the 3D US acquired images on the treatment day to the 3D US reference image on the planning day. Then the couch is shifted based on the tumor shift.

The drawback of this system is that it is suitable only for the prostate, which is affected by respiratory motion [53].

Sen HT et al. [53] have developed a robotic system to use during both simulation (SIM) and treatment delivery in the Linear Accelerator (Fig. 11). The probe could create deformations for soft tissues. To compensate for these deformations, the robot holds the probe on the patient during the planning CT imaging process, thereby ensuring that planning is performed on the deformed tissue. During treatment, the patient setup can be improved by using US imaging by visualizing the soft-tissue target, rather than by relying on the bony anatomy.

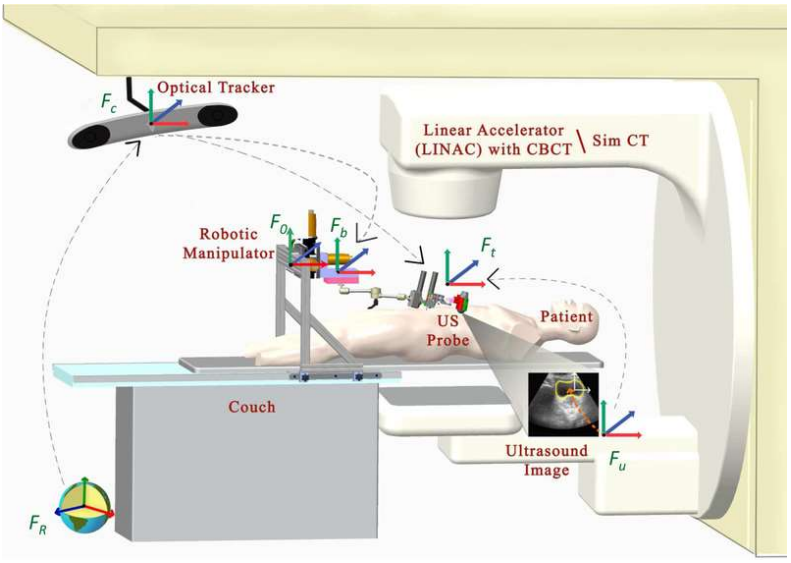

Fig. 11. Robotic US system [53]

1.4.4. Electromagnetic Tracking Systems

Other systems such as X-ray, CT, and MRI systems allow capturing only a snapshot of the organ motion, while the 4D localization systems provide real-time tracking of organ motion.

The Calypso® 4D localization system (Fig. 12) is an example of a continuous motion tracking system. This system uses a type of electromagnetic transponders. It is only limited to prostate cancer. Electromagnetic transponders can be implanted surgically into the prostate. The motion of these transponders can be detected by ceiling-mounted infrared cameras. These cameras are integrated with a detector array system that defines the prostate location and allows for continuous monitoring and evaluation of the intrafraction motion by resonant radiofrequency, which results in positioning the patient accurately during the treatment [51].

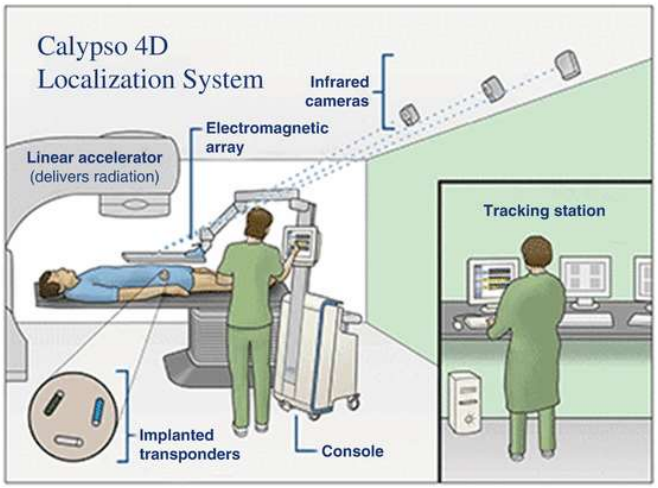

Fig. 12. The electromagnetic tracking system (Calypso, Varian Medical Systems) [29].

The advantages of this system are, using safe radiofrequency wavelengths (i.e: lack of ionizing radiation). The implanted transponders provide a superior temporal resolution which results in real-time tracking intrafraction motion, but there is no information about the deformation of prostate or critical normal tissue even motion of seminal vesicle nor motion of critical normal tissue [54].

1.4.5. Camera-Based (Infrared) or Optical Tracking Systems

There are two main types of optical tracking systems, the first one depends on using infrared cameras to track the motion, the second one depends on using video cameras for tracking or surface imaging.

These systems are useful for patient positioning and intrafraction monitoring, provide information on the external anatomy (requires knowledge of the relationship between the motion of the target and the external anatomy), non-invasive methods, require zero radiation dose. But the main disadvantage is that unable to visualize the soft tissue.

Recently, the estimating subsurface dose concept was established by imaging the intensity and distribution of Cherenkov light emission during radiation therapy such as the BrainLAB ExacTrac system. The emitted light has a low-intensity, broad-spectrum signal, dose-depositing electrons. Cherenkov imaging is a real-time technique. This system consists of a Cherenkov camera and optical surface guidance projectors and cameras which are fixed to the ceiling (Fig. 13). The linear accelerator gantry rotates to each beam position for delivery of each field. When the beam of linac (yellow) is incident the tissue, Cherenkov light is emitted isotropically from within. The emitted light can be detected by the Cherenkov camera (blue). The camera intensifier is triggered during only the linear accelerator pulses, thereby preventing interference with the ambient light. The optical surface guidance system cameras are used for patient set up and ensuring the correct alignment by exposing the patient to diffuse light pattern (red), and tracking movement [55].

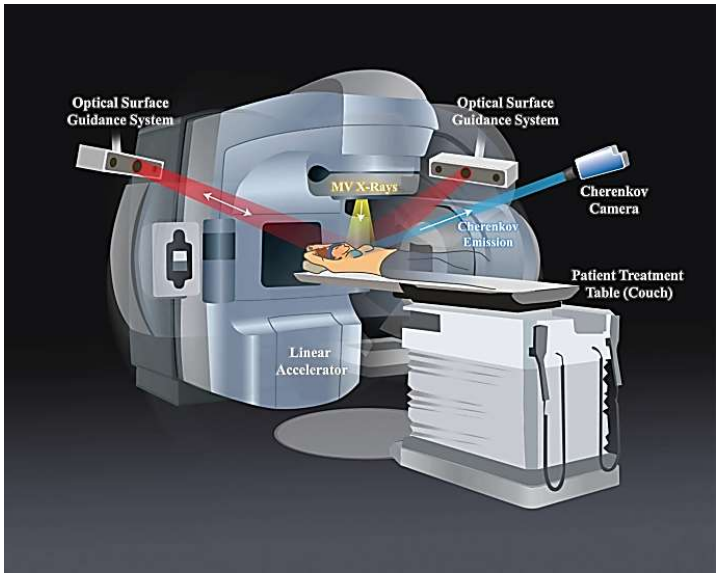

Fig. 13. Cherenkov imaging is a real-time technique [55].

1.4.6. MRI-Guided IGRT

Magnetic resonance imaging (MRI) has been introduced for IGRT in the last 10 years for imaging-guided radiotherapy (IGRT) and is known as MR-guided radiation therapy (MRgRT). The initial design of the integrated MRgRT unit is a combination of an MR scanner with a specially designed teletherapy machine. Newer units of MRgRT are linear accelerator-based (e.g MRIdian Linac, ViewRay) (Fig.14). MRI-Linac is a combination of an MRI unit and a 6 MV linear accelerator. It uses MRI for planning and image guidance [1]. This technique is useful for treating soft tissue tumors such as the liver, pancreas, kidney, and so on. MRI-guided RT can provide a detailed snapshot of the anatomy before treatment and able to track the target during the treatment as well [56].

The advantages of MRI-guided RT are the ability to image without using ionizing radiation, the superior soft-tissue contrast, especially for the central nervous system (CNS), abdomen, and pelvis, providing real-time assessment of internal soft-tissue anatomy and motion and allowing for intra-fractional corrections.

The disadvantages of MRI-guided RT are distortion with non-uniform magnetic fields, motion artifacts, and cannot be performed for patients with pacemakers or metallic implants.

Fig. 14. MRIdian Linac, ViewRay [57]

1.5. Image quality assessment (IQA)

Image-guided radiotherapy (IGRT) systems are usually used to assess patient positioning, localize targets and organs at risk before or at the time of treatment through image registration to minimize geometric uncertainties. The large cone angle in technologies that are based on cone-beam geometry such as MV-CBCT and kV-CBCT allows x-ray scatter to contribute undesirable signals by reducing soft-tissue contrast, increasing image noise, introducing artifacts, and reducing the reconstructed CT number accuracy [58]. As result, the image quality is affected by blurring.

The imaging performance of these systems relates to how well an image is resolved and how well it provides the anatomy and functional information to the physician. Therefore, the image quality of these systems is a vital factor and a characteristic used to evaluate the imaging performance. The imaging performance can be evaluated through testing ten different parameters by using commercially available phantoms that contain multiple inserts tailored to test various aspects of image quality [58]. These tests included: 1. Slice Thickness Verification, 2. Spatial Linearity (Geometric Verification), 3. Pixel Size Verification, 4. Spherical Contrast Target Evaluation, 5. CT Number Accuracy, 6. Spatial Resolution, 7. Low Contrast Detectability, 8. Contrast-to-Noise Ratio (CNR), 9. Artifact Evaluation, and 10. Image Uniformity.

The AAPM TG-179 recommends that during system acceptance, the image quality tests be performed to obtain a system performance baseline that can be compared to quality assurance (QA) results acquired under identical conditions. This section describes the general principles of some of these tests.

1.5.1. Hounsfield Unit (CT Numbers)

The x-ray beam attenuation in CT depends on the composition of the tissues (physical density and atomic number) and the thickness of the anatomy [59]. After reconstruction of the CT image, each pixel (picture element) is represented by a number, which is a rescaled normalized value of the calculated X-ray absorption coefficient of a pixel [59]. This number is called a CT number and can be represented by a specific unit called the Hounsfield unit (HU). For water, the Hounsfield unit value is 0 HU and for air is −1000 HU at all tube energies used. CT number or HU are calculated as follows [60]:

$$HU = \frac{\mu t - \mu w}{\mu w - \mu air} * 100 \quad (1)$$

Where μ_t, μ_w, and μ_{air} are the absorption coefficient of tissue, water, and air, respectively. Since the μ_{air} is negligibly small, therefore, Eq. 1 can be written as:

$$HU = \left[\frac{\mu t - \mu w}{\mu w}\right] * 100 \quad (2)$$

1.5.2. Image Uniformity

Uniformity is defined as the ability of the CT scanners to produce an image of a homogeneous object with mean pixel values that do not depend on the position of the pixel (over several small regions of interest (ROI). In the ideal case, the images have the same quality across the whole of the image. But uniformity is usually unachievable due to beam hardening and other artifacts. Therefore, testing

uniformity is an essential quality control (QC) test and should be performed at acceptance and once a month then [61]. The degree of uniformity determines the accuracy of CT number measurement.

The difference in the mean CT number between a peripheral (edges) and a central region of a homogeneous test object should be ≤8 HU [62].

1.5.3. Contrast

In general, an image can be described as a good contrast if the darker parts are darker, and the lighter parts are lighter. In CT, the image contrast can be determined by measuring differences between the object density and its background (in CT numbers). Contrast can be expressed mathematically in terms of a percent difference in CT numbers (ΔCT (%)) as given in Eq. 3:

$$\Delta \mathrm{CT}\ \% = \left[\frac{\left|\mathrm{CT2} - \mathrm{CT1}\right|}{1000}\right] * 100 \qquad (3)$$

A big difference in CT numbers corresponds to good contrast [62].

1.5.4. Resolution

Resolution is defined as the ability to distinguish small objects with high contrast (high HU unit) as well as to distinguish between small objects very close to each other (low contrast). Spatial resolution is interdependent at high contrast and low contrast. Resolution is considered an important factor for image quality. The spatial resolution at high contrast determines the minimum size of detail visualized in the plane of the slice. It is influenced by factors such as detector width, slice thickness, pixel size, the field of view (FOV), X-ray tube focal spot size, object-to-detector distance. The spatial resolution at low contrast determines the size of detail that can be visibly reproduced in case of existing only a small difference in density relative to the surrounding area. It is affected by dose and image noise.

1.5.5. Noise

In general, every measurement is associated with a certain margin of error, and all measured values fluctuate around the true value. In CT the value that is measured is the attenuation caused by body parts or tissues, represented by its Hounsfield (HU) value. Each volume element (voxel) of a CT image is a measurement of the respective attenuation caused by the scanned object. Therefore, if a CT scan of the same object is repeated, the scan will always yield a slightly different CT value for this voxel. If a homogeneous object such as a water phantom is scanned, each voxel in the image can be interpreted as an independent measurement of the same material. Thus, a CT scan of a homogeneous object can be interpreted as many independent measurements of the same material carried out at the same time. All voxel values will fluctuate around the true value of the object, for example, water or tissue. The measurement error is directly visible in the image and is usually called image noise. If a sufficiently large number of measurements are carried out, the average of the measured values is close to the true value. In a CT image, the image noise and the true HU value can be estimated by evaluating a sufficiently large homogeneous region of interest (ROI) in the image and calculating the standard deviation of the CT numbers.

1.5.6. Slice Thickness

Slice thickness affects the quality of the image because of variation in noise due to slice thickness. Thin slices are noisier. Therefore, soft tissue contrast is lost if the slice is too thin. For bone contrast, due to the existence of greater image contrast, the bone contrast is not affected by slice thickness.

1.6. Imaging protocols analysis

The use of Cone-beam computed tomography (CBCT) in image-guided radiation therapy (IGRT) has three main roles in clinical use: patient setup verification and position adjustment, tumor localization, and tumor changes tracking during treatment. Nevertheless, there are concerns regarding using CBCT in clinical use, mainly related to the increased scatter contribution, the imaging artifacts, and overall image quality as mentioned in the previous chapter [63].

The use of CBCT in IGRT has enhanced the radiation treatment by providing accurate patient position spatial information. However, various studies have reported on the dose from CBCT showing the risks of secondary cancer [38]. Therefore, it has led to improve CBCT scanning protocols by lowering the dose at the expense of compromising spatial resolution. Although the delivered dose to patients in CBCT is significantly higher than that of fan-beam CT, the healthy tissue is received a lower dose.

Srinivasan et. al, [38] stated that with improved HU uniformity, CBCT datasets could be directly used for treatment planning without the need for a planning CT.

The reconstructed CBCT images can be used to correct patient position before treatment or as a basis to adapt the treatment plan to the changing anatomy of the patient during radiotherapy.

The use of Cone-beam Computed Tomography (CBCT) in radiotherapy is increasing due to the widespread implementation of kilovoltage systems on the currently available linear accelerators. Cone beam CT acts as an effective Image-Guided Radiotherapy (IGRT) tool for the verification of patient position.

1.6.1. CBCT imaging protocols analysis:

Yan H et al. [64] suggested that for a given low dose level, the best image quality can be acquired by using a medium mAs/view level and a medium number of projections which is known as the optimal scan protocol. Based on their results, the optimal number of projections is around 90 to 120. In this study, the safe dose level for the low-contrast objects visualizing is stated as 72.8 mAs, while the sufficient dose level for detecting high-contrast objects of diameter ~ 3 mm is 12.2 total mAs.

2. Materials and Methods

Cone-beam computed tomography (CBCT) is an effective Image-Guided Radiotherapy (IGRT) tool for the verification of patient position where CBCT is used to assess patient positioning at the time of treatment through image registration. Therefore, image quality (IQ) parameters of these devices, such as image uniformity and noise, spatial resolution, resolution, contrast-to-noise ratio, are of great importance. AAPM strongly recommends periodic evaluation of image quality (IQ) [65]. To meet the recommendation, the evaluation of IQ can be performed by using a phantom specifically designed for such tests. Procedures of Image quality parameters measurements are explained in this chapter.

2.1. Data acquisition

2.1.1. Linac systems - *Halcyon* Imaging System - Treatment device and imaging modalities

The *Halcyon* is a new machine from a Varian supplier (Varian Medical Systems, Palo Alto, CA) that recently has been installed in the Hospital of Lithuanian University of Health Sciences Kaunas Clinics, Oncology Hospital, Radiotherapy department (Fig.15). The *Halcyon* is designed for intensity-modulated radiation therapy/volumetric modulated arc therapy (IMRT/VMAT). It consists of a linear accelerator (LINAC) mounted on an O-ring gantry (bore-enclosed linear accelerator) (Fig. 16) which produces a single 6 MV flattening filter-free (FFF) photon beam delivering a maximum dose rate of 800 MU/min under calibration conditions as mentioned by S. Panda et al. [66] This beam is used for both treatment and imaging. The kV imaging system is orthogonal to the MV beamline and Opposite to the kV x-ray source, a large imaging panel (an amorphous Si detector) with dimensions 43 ×43 cm with 0.336 mm pixel pitch in each dimension is fixed at a source-to-imager distance of 154 cm (Fig.17). The panel is operated at 25 frames/sec at full resolution to enable capturing at a high dose rate without saturation.

Fig. 15. The *Halcyon* radiation treatment system.

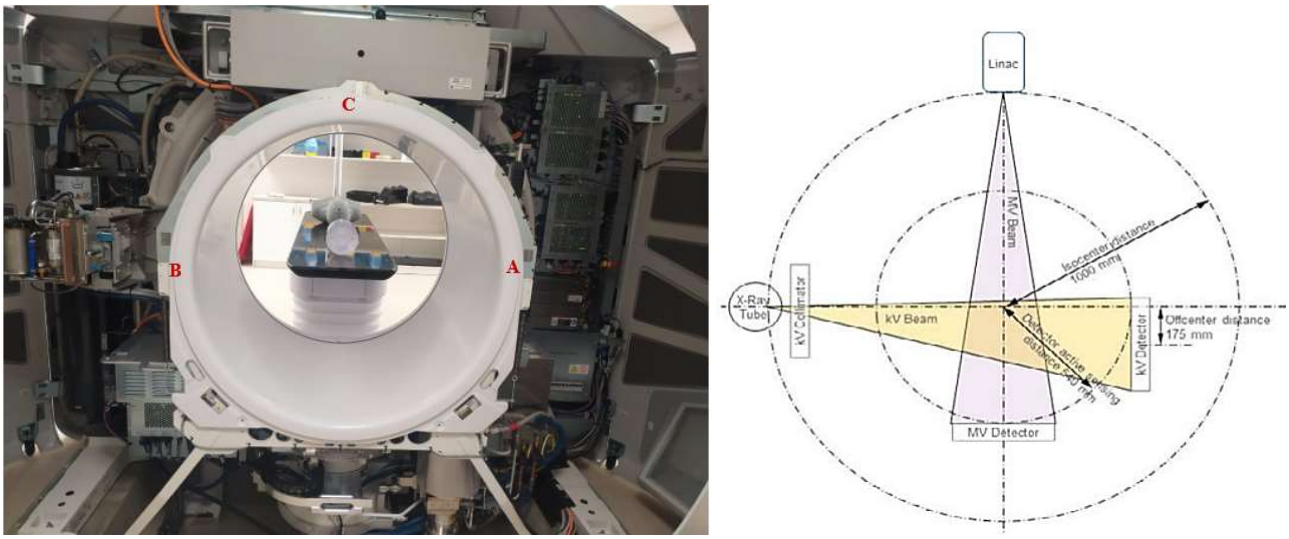

Fig. 16. External view of the *Halcyon* system with 1m bore size diameter and Internal view of fixed kV source "A", kV detector "B", and MV beamline "C"; kV and MV beamline arrangement (image on the right) [67]

The maximum field size or the maximum field of view FOV at the isocentre (1 m) (28 * 28 cm^2) is defined by a dual-layer multi-leaf collimator (MLC) system. The jawless MLC is composed of two staggered layers of 28 leaf pairs, with a projected leaf width of 1cm at isocentre without light field, front pointer mechanism, optical distance indicator, or physical jaws. The maximum leaf speed and the leaf span are 5 cm/s and 28 cm respectively.

Patient setup is performed by aligning to lasers mounted to the front of the bore Fig.17 and then the patient couch is shifted to loading to a virtual isocentre [67]. Positioning is verified through MV imaging with kV imaging [68].

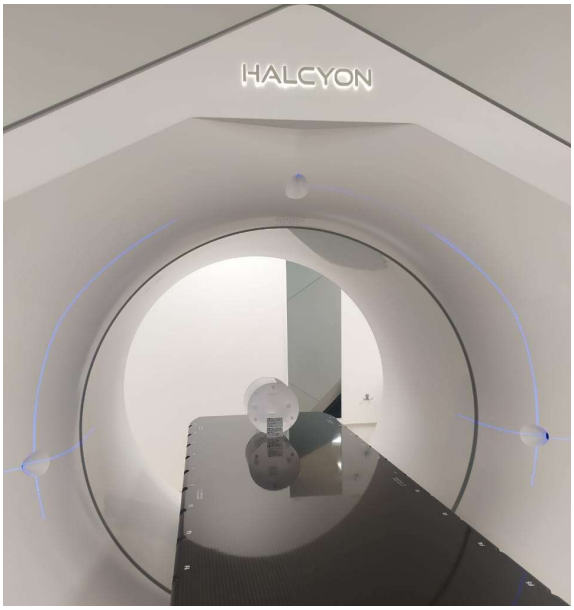

Fig. 17. Laser system mounted to the front of the bore.

The main features of the *Halcyon* linear accelerator are summarized as, jawless design, faster gantry rotation in both imaging and delivery mode /4 rotations per minute (RPM), a dual-layer multi-leaf collimator (MLC), and automated daily image-guided radiotherapy (IGRT) [68].

One of the key innovations in the *Halcyon* system is the kilovoltage (kV) IGRT imaging system. The kV system has several features, that allow this system to be more robust IGRT, such as the fast acquisition of kV cone-beam computed tomography (kV CBCT), large field-of-view (FOV), and extended scan range.

Halcyon system also has Megavoltage cone-beam computed tomography (MV CBCT) capabilities using the same 6 MV flattening filter-free beam used for treatment. This system is also capable of MV portal imaging.

The *Halcyon* system for this research work has been used to acquire CBCT images of the used phantom.

2.1.2. KV CBCT imaging protocols:

Kilovoltage volumetric CBCT imaging is available with eleven scanning protocols for clinical use. The scanning protocols are described by Cai et al. [69] where a full 360° trajectory is used for all kV imaging protocols but with a different number of projections where it ranged from 463 to 895 projections. The diameter of the scanned FOV is ranged 28.1to 49.1 cm.

Fixed scanning energies (80, 100, 125, and 140 kV) are utilized for preset imaging protocols but with different adjustable mAs settings. The measured slice thickness of a reconstructed image depends on the used reconstruction algorithm.

The scanning time is short (16.6 sec) for only six protocols, where the remaining five protocols are used large scanning times ranged from 21.1 to 40.6 sec depending on the delivered dose and number of projections.

In this study, we evaluate the performance of the IGRT system (for the linear accelerator *Halcyon*) by the implementation of imaging QC tests to assess the performance of KV images.

2.1.3. Phantom

2.1.3.1. Phantom Quart

Phantom *Quart* (model: Quart DVT _VN CBCT, Quality Assurance In Radiology “QUART” GmbH) [70] has been used for image quality evaluation of MV/KV CBCT reconstructions. The phantom is made of PMMA (Acrylic) with a diameter of 160 mm. Its design is simple and lightweight. The phantom is transparent with visible white cross markers for laser alignment (Fig. 18).

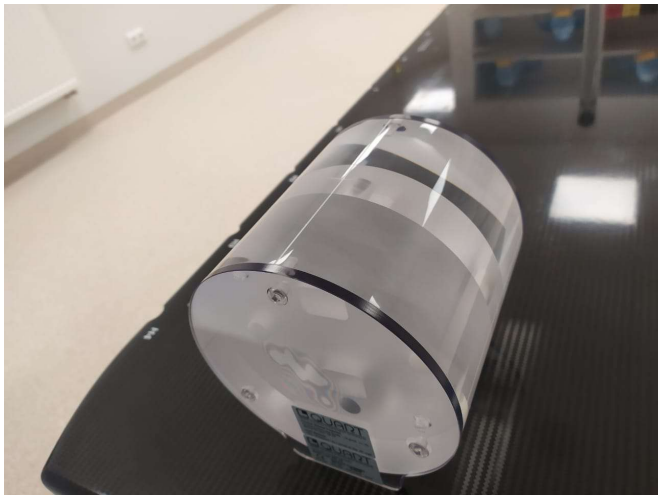

Fig. 18. phantom *QUART DVT_VN*.

The phantom composed of several modules:

- A central 3 cm thick module containing four cylindrical holes of 15 mm diameter and their centers are at 25.5 mm radius from the centers of the phantom. Two of these holes are empty (air), 1 hole contains PTFE (Teflon) cylindrical insert, and 1 hole contains Polystyrene cylindrical insert (Fig. 19). The central thick module also contains two rectangular inserts containing 0.5 mm thick tilted air gaps inclined 30̊ for measuring slice thickness (28 mm wide and 20 mm high, and their centers are 32.25 mm above and below the phantom centers.
- Two identical, 6 cm thick homogeneous PMMA modules. These modules are used as uniformity modules and provide scattering material on both sides of the central modules. By existing these modules, the phantom is well adapted to CBCT applications. Without these modules, systematic errors in HU values can occur. Table 1. demonstrates the nominal HU values of phantom materials provided by the manufacturer [70].
- Two, 6 cm thick polycarbonate plates on both faces of the cylinder for stable positioning of the phantom on the couch surface.

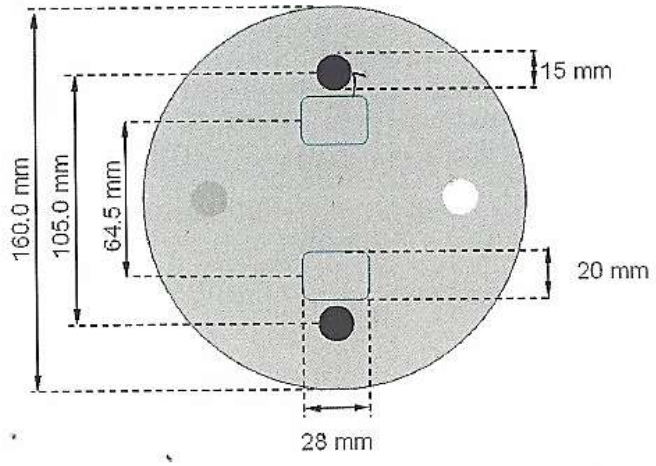

Fig. 19. A schematic drawing of the central module of the phantom *QUART* [70]

Table 1. The nominal HU values of phantom materials [70]

Material types	Nominal HU value
PMMA (Acrylic)	+120
Polystyrene	-35
PTFE (Teflon)	+990
Air	-1000
Water	0

To collect all necessary parameters to determine the imaging quality for the equipment being tested, only one exposure is required. After the exposure, the image is evaluated by a treatment planning system (TPS) and tools of the software *ImageJ* (National Institute of Health, USA) [71].

After positioning the phantom, scanning is initiated. The software will collect data from the test images and create a test protocol. The whole procedure (including phantom positioning, evaluation of software-assisted, and test protocol creation) takes approximately 5 minutes.

2.1.3.2. Tissue Characterization Phantom - Phantom *Gammex 467*

The *Gammex 467* Tissue Characterization Phantom is used to establish the relationship between the electron density (ρ_e) of different tissues and their HU values. Such information is useful in CT image reading for accurate corrections for tissue heterogeneities.

The *Gammex 467* is composed of a 33 cm diameter Solid Water® disk (~ the size of an average pelvis). A matrix of sixteen holes with a diameter of 2.8 cm in the disk holds interchangeable rods of various tissue and water substitutes (Figure 20). The electron density relative to water of the rod materials and physical density (g/cm^3) are listed in Table 2 with a corresponding graph in Figure 21.

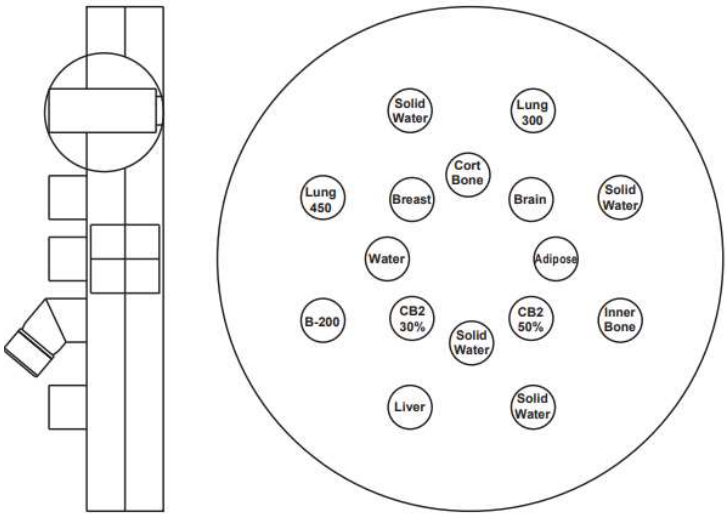

Fig. 20. The cross-section of phantom *Gammex 467*

Table 2. Nominal electron and physical densities of Materials of phantom *Gammex 467*

Rod Materials	Physical density, g/cm^3	Electron density relative to water
LN-300 Lung	0.290	0.286
LN-450 Lung	0.480	0.463
AP6 Adipose	0.944	0.927
BR-12 Breast	0.984	0.961
Water Insert	1.000	1.000
CT Solid Water1	1.015	0.986
CT Solid Water2	1.015	0.986
CT Solid Water3	1.015	0.986
CT Solid Water4	1.015	0.986
BRN-SR2 Brain	1.052	1.048
MS11 Muscle	1.052	1.021
LV1 Liver	1.093	1.061
IB Inner Bone	1.134	1.087
B200 Bone Mineral	1.142	1.095
CB2-30% CaCO3	1.332	1.277
CB2-50% CaCO3	1.559	1.469
SB3 Cortical Bone	1.810	1.683
Titanium Grade 2	4.590	3.790
316 St Stl	8.000	6.580

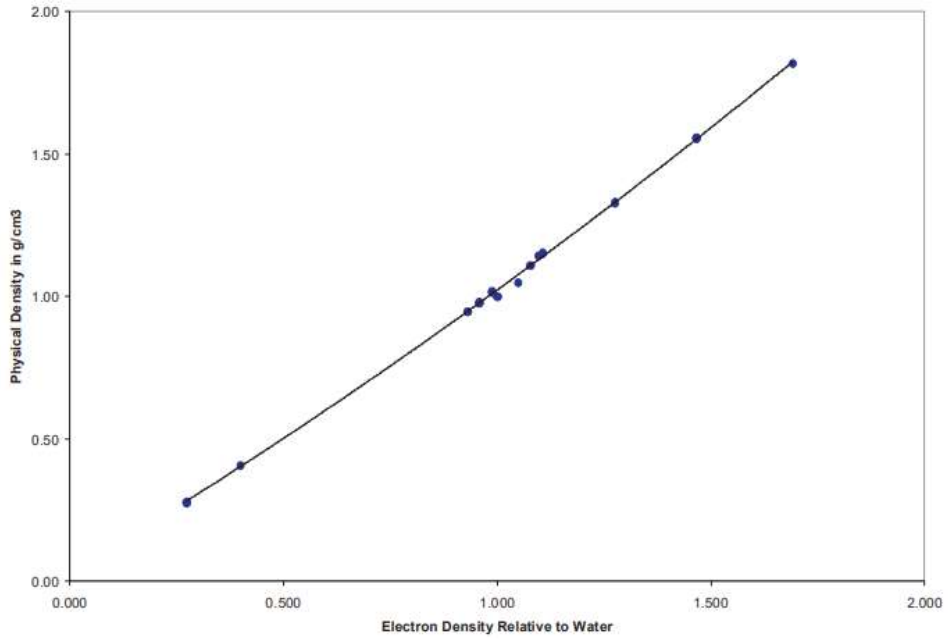

Fig. 21. The relation between density and electron density relative to water of tissue substituting materials in the phantom *Gammex 467*

A pattern of eight holes with a diameter of 1 mm and 50 mm spacings are positioned around the phantom center as shown in fig. 22, To assist in checking the accuracy of the scanner.

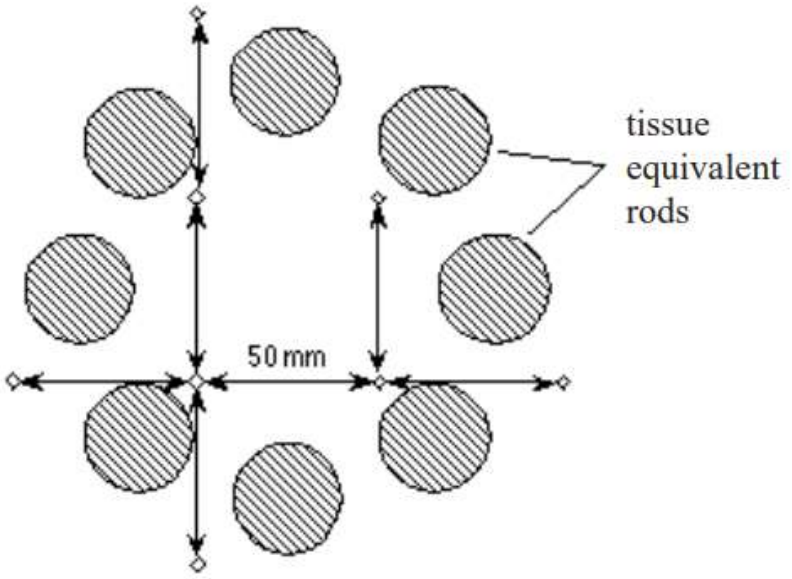

Fig. 22. Airhole pattern (50 mm holes spacing).

It is important to distribute rods with the high-density tissue substitute throughout the phantom equally to minimize artifacts. A recommended rod arrangement is shown below (r = ρe w) (fig.23).

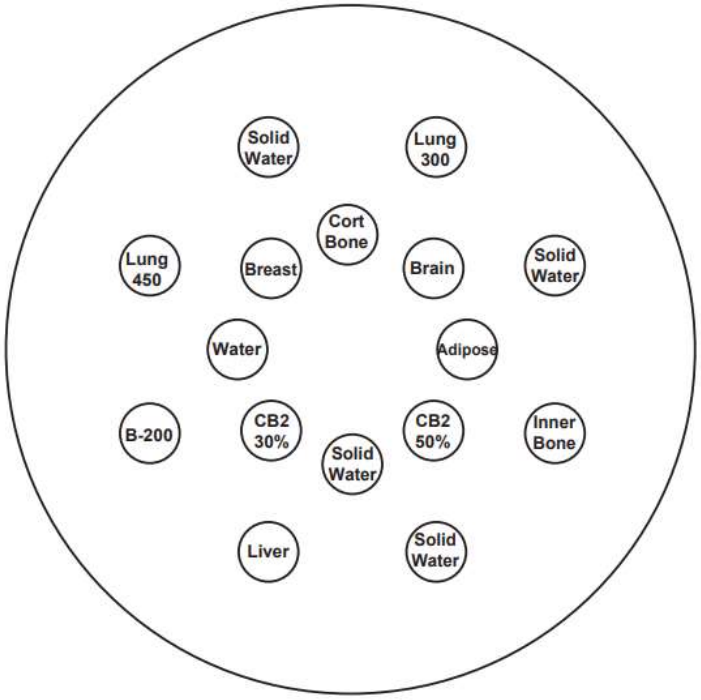

Fig. 23. Suggested arrangement of tissue substituting rods

2.1.4. Treatment planning system *Eclipse*

The commercial treatment planning system (TPS) evaluated in this study is *Varian Eclipse* (Varian Medical Systems, Palo Alto, CA, USA).

2.2. Implementation

The *Halcyon* system has been used to acquire CBCT images of both phantoms *QUART* and *Gammex 467*.

2.2.1. Phantom *QUART* Alignment

For phantom *QUART*, a laser system has been used to align the grooves on the phantom, which are outlined in white color for better visibility (Fig.24). The phantom is transparent, therefore internal structures are visible, which also simplifies the alignment. The phantom is symmetric where both orientations are equivalent (except the location of Teflon and Polystyrene inserts).

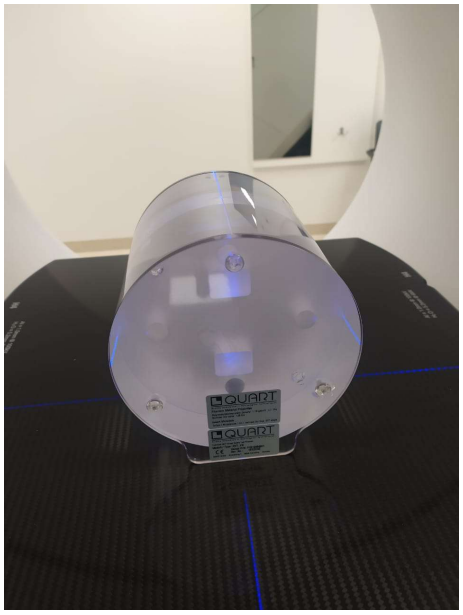

Fig. 24. Aligning of *QUART* phantom using laser on Halcyon system

After the phantom had been positioned in the scan center, the exposure is initiated. After the exposure, CBCT images have been acquired, DICOM slice images are directly loaded into the *Eclipse*. The *Eclipse* will guide the evaluation process. The image's average and standard deviation have been calculated for each evaluation of image quality.

The central slice of a thorax 125 kV scan of phantom *QUART* was acquired by using *Halcyon* as shown in Fig. 25. left). The central slice of MV-CBCT high-quality scan (6 MV FFT) of phantom *QUART* was acquired by using *Halcyon* as shown in Fig. 23. right). The left and right circular areas are the Teflon and Polystyrene inserts and the two dark lines between the top and bottom air holes represent the air gap that is used to measure slice thickness. As expected, and mentioned in chapter one, the image quality of MV-CBCT is lower than that of KV-CBCT.

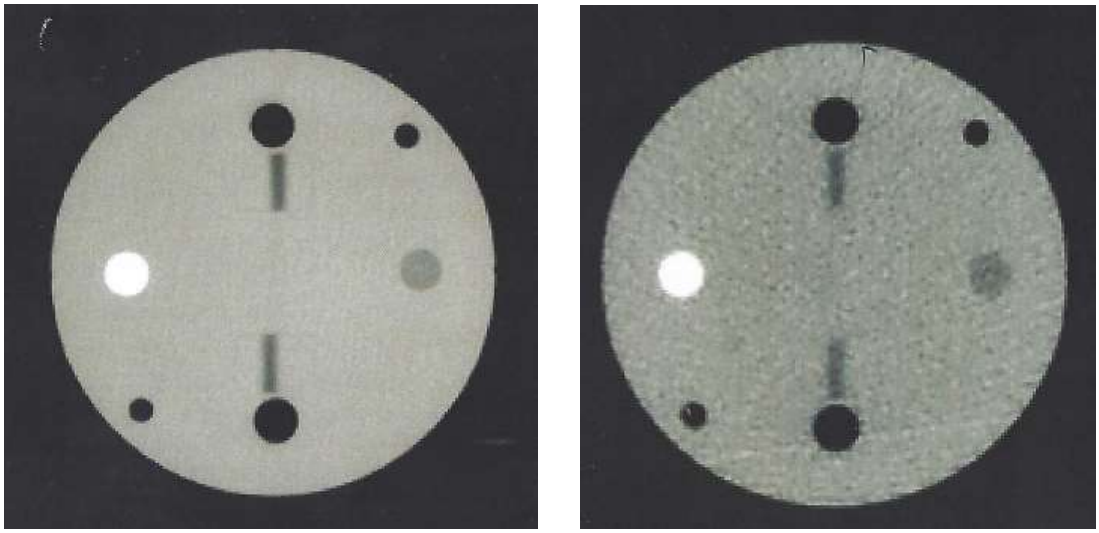

Fig. 25. KV-CBCT scan (image on the left), MV-CBCT scan (image on the right), of the phantom *QUART* [70]

2.2.2. *Gammex 467* Phantom Alignment

The phantom has been Placed (standing on its side) onto the gantry and positioned by aligning the crosshair decals with the lasers. A circumferential line has been Used to scan a slice through the center of the phantom.

2.3. Image quality assessment (IQA)

The image quality has been evaluated on the Halcyon system using a *QUART* phantom and *Gammex 467* phantom. CBCT reconstruction data are provided as HU values. The following parameters have been selected and measured for image quality control of CBCT devices: HU accuracy, uniformity, noise, slice thickness, and geometric scaling.

2.3.1. HU Accuracy measurement

The HU accuracy of a CBCT reconstruction can be evaluated by measuring the mean HU values of *QUART* phantom in various regions of interest (ROIs) that have different materials such as bulk material (Acrylic), Teflon, Polystyrene as well as the two air holes can also be used.

In this test, a well-centered slice has been selected. The selected slice has been managed by using the TPS (*Eclipse*) which allows measuring of the average HU value in the selected ROIs. Three different materials that have been used are Teflon, Polystyrene, and air. By using the *Eclipse*, a circle ROI has been drawn in each selected material as shown in Fig. 26 in blue color. A small margin has been left around the insert boundaries, where the diameters of the ROIs are smaller than the diameters of inserts which is 15 mm (i.e.: the diameter of all ROIs is approximately 12 mm). The measured mean values that are obtained by the *Eclipse* have been compared with the nominally expected values mentioned in Table.1. The differences between the measured average and nominal expected values are known as HU accuracy.

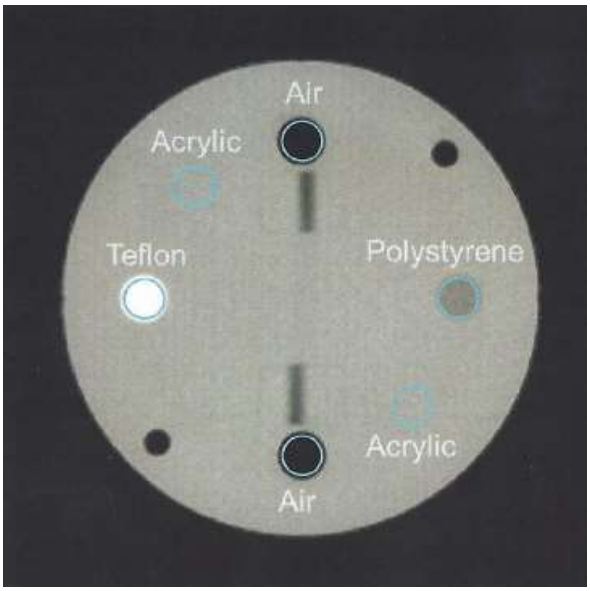

Fig. 26. *QUART* phantom Central slice of CBCT reconstruction of HU accuracy-test module. ROIs are shown in the blue circle [70].

After scanning the *Gammex 467* phantom, the spacing of the eight 1 mm air holes has been measured by using *Eclipse* to check the accuracy of the scanner's caliper. The holes are spaced 50 mm apart (as shown in fig. 23). A 1 cm diameter Region of Interest (ROI) has been selected. The HU value for each rod has been measured and recorded. The HU value at several different points in the Solid Water disk has been recorded, considering the distance of each ROI from the center of the disk (Fig. 27).

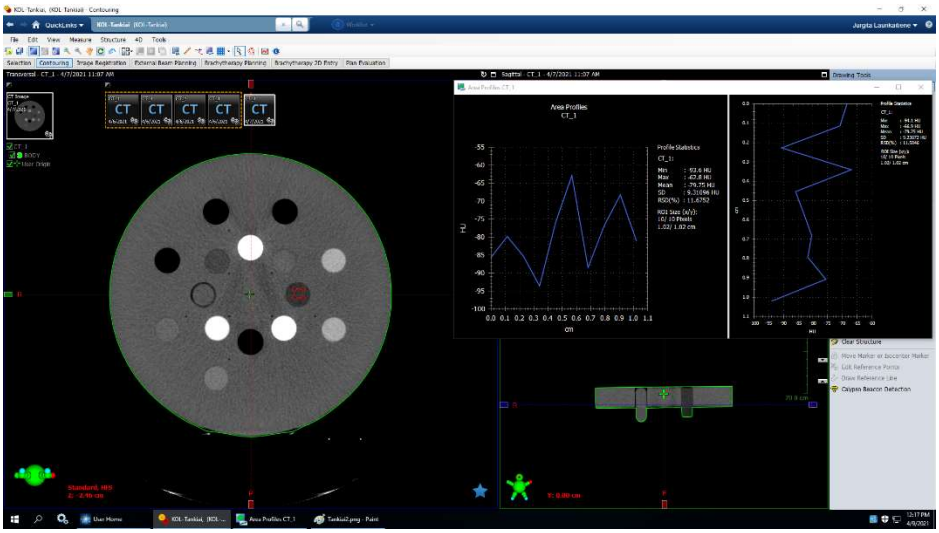

Fig. 27. *Gammex 467* phantom slice of CBCT reconstruction of HU accuracy-test

2.3.2. HU uniformity measurement

The HU uniformity of a CBCT reconstruction can be measured in one of the two 6 cm thick homogeneous modules that are on each side of the central module. The measurements have been done by selecting a slice in the homogeneous area as shown in Fig. 28. Different five small ROIs have been created, one at

the center and four peripheral regions of the phantom by using Eclipse. The drawn squares with a length of 15 to 20 cm are to limit the influence of local noise.

HU uniformity is given by the maximum difference between all HU average values of the different ROIs in absolute HU values.

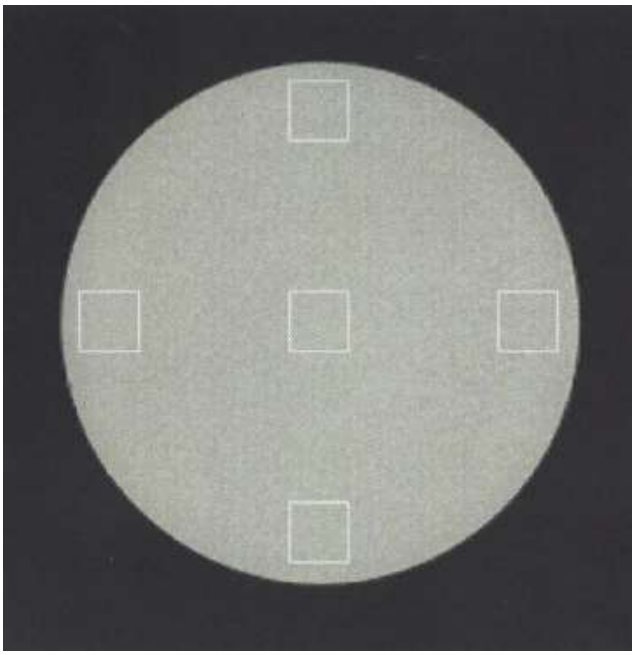

Fig. 28. phantom *QUART* Homogeneous region of CBCT and the reconstructed slice of HU uniformity test module.

2.3.3. Noise, SNR, and CNR measurement

Noise in the image was calculated using the standard deviation of the pixel values divided by the mean values in the ROIs. These ROIs can be selected in the homogenous slice, or the central slice of the phantom as shown in Fig. 29.

Single-to-Noise Ratio (SNR)

The real signal is defined as the signal that expresses the anatomy of the region of interest. The noise signal is defined as the amount of signal that is created due to random scattering effects. It is important to not consider the level of image noise only but to consider the ratio of the real signal to the noise signal as well. When the signal-to-noise ratio (SNR) is decreased, a grainier image will be produced. In general, CBCT images have relatively more noise from scattering due to the cone geometry is large.

Noise in the image is given by using the standard deviation of the HU values in a selected ROI, and the signal is given relative to air. SNR can be calculated by using the following formula:

$$\mathrm{SNR} = (\mathrm{HU\ value} + 1000)/\sigma \qquad (4)$$

where σ refers to the standard deviation.

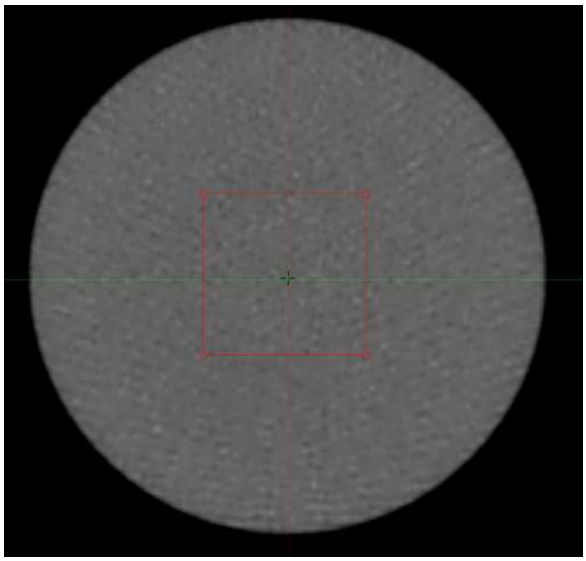

Fig. 29. Phantom *QUART* and the reconstructed image of the noise test module.

Contrast-to-Noise Ratio (CNR)

The low contrast detectability depends on the amount of noise in the image. One way of quantifying the contrast in an image is by determining the contrast-to-noise ratio (CNR). The value of CNR describes the quality of an image and can be given by calculating the difference of HU values between a certain insert and the material surrounding it, divided by the noise (Eq. 5).

$$\mathrm{CNR} = \frac{[\mathrm{abs}\ (\mathrm{HU\ insert} - \mathrm{HU\ background})]}{\sqrt{\sigma 2\ insert + \sigma 2\ background}} \quad (5)$$

where $\mathrm{HU}_{\mathrm{insert}}$ is the mean HU values over an ROI in an insert and $\mathrm{HU}_{\mathrm{background}}$ is the mean HU values over an ROI in the background, and σ_{insert} and $\sigma_{\mathrm{background}}$ is the standard deviations of the HU values in an ROI in the background. In general, the larger the CNR, the less noise is viewed in an image and the quality is improved. The images which have a great amount of noise are the images with the lowest CNR value.

2.3.4. Low contrast variability (LCV) measurement

Another factor of image quality to consider is the ability of a system to detect low visibility objects or objects with different contrast. To measure the image quality, it should define a value known as low contrast visibility (LCV). In a study that was done by Elstrøm, et al. [72] two inserts with small differences in mass density and HU values, low-density polyethylene, and polystyrene, were placed in the phantom. Where the mass density of low-density polyethylene and polystyrene are (-100 HU and -35 HU) respectively and the HU values are (1.05 g/ cm^3 and 0.92 g/cm^3) respectively. From this measurement, the LCV was calculated by using the following equation (Eq. 6):

$$\mathrm{LCV} = \frac{2.75(\sigma 1 + \sigma 2)}{\mathrm{P1} - \mathrm{P2}} \quad (6)$$

Where σ1 is the standard deviation of a region of interest inside the polystyrene insert, and σ2 is the standard deviation of a region of interest inside the polyethylene insert, P1 is the mean pixel value of a region of interest inside the polystyrene insert, P2 is the mean pixel value of a region of interest inside the polyethylene insert.

The low contrast variability value becomes small if the noise is at a low level. The smaller the low contrast variability, the better differentiation between regions, and good contrast is present. For the evaluation, five locations in inserts have been selected and the mean and standard deviation (SD) was calculated.

2.3.5. Slice thickness measurement

The measurement of slice thickness is based on evaluating the shape of a tilted structure in a single constructed slice. The slice thickness can be determined by taking a profile and measuring the full width of half maximum (FWHM). Where the effective slice thickness (s) is given by Eq .7.

$$S = \tan(\alpha) * FWHM \quad (7)$$

In phantom *QUART*, the slice thickness is measured using an inclined air gap. The phantom *QUART* has an air gap of 0.5 mm in width. The inclination angle is 30̊, therefore the slice thickness can be given by Eq. 8.

$$S = 0.577 * FWHM \quad (8)$$

In this test, a well-centered slice with an air gap has been selected. The ROI has been defined (20 mm high) (Fig. 30). The horizontal profiles around the air gap have been calculated using ImageJ software.

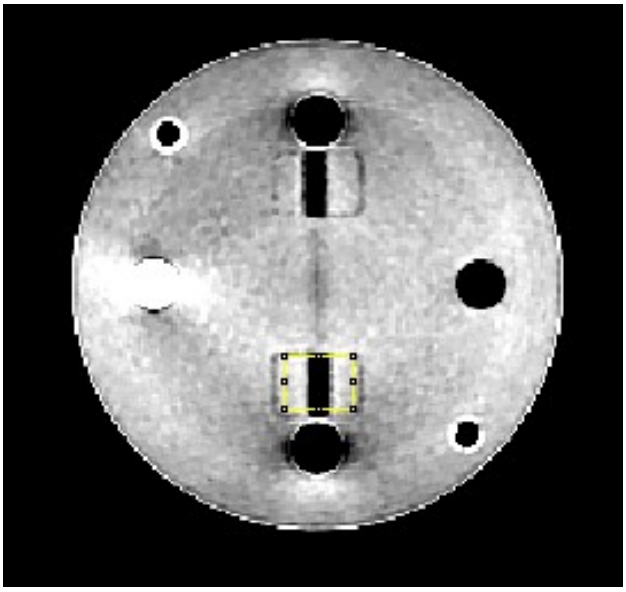

Fig. 30. The phantom *QUART* Central slice of CBCT reconstruction of slice thickness test module.

2.3.6. Geometric scaling measurement

The *Quart* phantom has a diameter of 160 mm. The geometric scaling can be verified by measuring the diameter both in horizontal and vertical directions. For a scaling measurement based on the diameter measurement, the accuracy is typical of the order of 1%.

3. Results and discussions

Image quality QC used for the daily routine as, the CBCT radiotherapy modalities recommendations are based on measurements and evaluation of the constancy of these quality parameters of the image, concerning a baseline for the used protocols, and there are no established action levels [73]. Some authors suggest using the baseline obtained at acceptance plus or minus three times the standard deviation as tolerances [74]. The baseline values of the different image quality parameters should be obtained over several scans with the same conditions as an average over different slices.

In this section, the evaluated image quality parameters have been measured, recorded, and analyzed for the kV CBCT modes using TPS (*Eclipse*) and image analysis software (*RadiAnt DICOM viewer*, and *ImageJ*) by following the phantom manufacturer recommendations.

3.1. HU Accuracy measurement

The values of the measured HU average of ROIs of a CBCT reconstruction slice have been measured by using the TPS (*Eclipse), RadiAnt*, and *ImageJ.* For Accuracy measurements and to avoiding any error occurring, the Aprile measurements have been repeated in May.

All measured values have been compared with the nominally expected values of the materials of these ROIs in the selected protocol as shown in Table 3 and Fig. 31. The results show correspondence HU values measured experimentally with known theoretical values, especially in the air gap regions. Comparing measured HU values that were obtained by TPS in April and May, the May results show more correspondence value than Aprile results especially for Polystyrene where the value of HU was -21 in April and -32 in May while the theoretical value is -35.

Regarding the software that was used for image evaluation the *ImageJ* and *RadiAnt* have shown better results for air gaps and Acrylic more than other materials.

Table 3. HU values of different ROIs

Materials	Polystyrene	Teflon	Acrylic	Acrylic	Air gap 1	Air gap 2
Theoretical HU average	-35	990	120	120	-1000	-1000
Measured HU average by using TPS (April)	-21	1151	170	181	-973	-980
Measured HU average by using TPS (May)	-32	1021	145	159	-986	-996
Measured HU average by using RadiAnt DICOM viewer	-23	1024	132	132	-999	-999
Measured HU average by using ImageJ	-29	1039	137	130	-999	-998

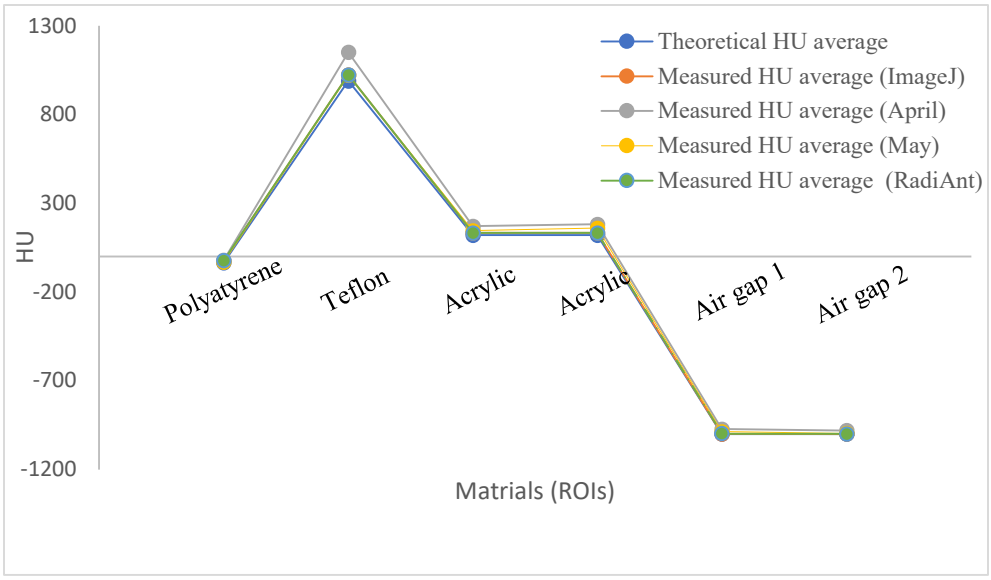

Fig. 31. A comparison between the measured and theoretical HU values of the different materials

The HU accuracy values of these ROIs have also been listed in Table 4 and plotted in Fig. 32. The highest calculated percentage differences errors were 51%, 42%, and 39% for Acrylic and Polystyrene respectively in April measurements by using TPS *Eclipse* while the lowest percentage was 0.2%, and 0.1% for air gap regions by using both image analysis software (*RadiAnt* and *ImageJ*). However, all accuracy results were accepted, but the results obtained by *RadiAnt* and *ImageJ* show a clear trend where the results were more accurate in all ROIs. Therefore, these software's could be successfully used for the results analysis, just due to the possibility to use commercially available system *Eclipse* this systems will be used for a clinical practice. The main goal of quality control is not to explain these differences, but to account for them when performing tests. Therefore, these results have been used to define a set of tolerance ranges for the HU of each material.

Table 4. HU accuracy values of different ROIs during performed monthly

Materials	Polystyrene	Teflon	Acrylic	Acrylic	Air gap 1	Air gap 2
Diff. % TPS (April)	39	16	42	51	3	2
Diff. % TPS (May)	9	3	21	33	1	0.4
Diff. % (RadiAnt)	34	3	10	10	0.1	0.1
Diff. % (ImageJ)	17	5	14	8	0.1	0.2

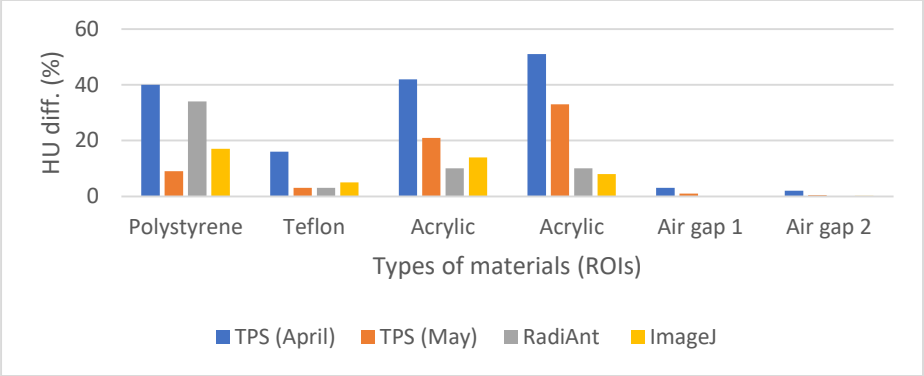

Fig. 32. HU accuracy values of different ROIs by using *Eclipse, RadiAnt*, and *ImageJ*

Additional measurements have been done using commercial phantom *Gammex 467*. The HU values have been measured, recorded in Table.5, and plotted in Fig.33 and Fig.34 vs. theoretical HU values and electron density relative to water (ρ_e^w) respectively.

The curves obtained in Fig.33 have been split into two regions, region for materials with a density below 1.1 g/cm^3 and region for materials with density higher than 1.1 g/cm^3. The difference between the measured HU and the theoretical value of HU. It was noticed that there is a large deviation between both values due to the high density of the materials (registered deviations were 0.66% to 27.5% for substitute materials of the lung, breast, brain, and liver and were in the range of 38.4% to 49.2 for bone substitute materials).

Table 5. Nominal Electron/Physical Densities, theoretical and measured HU of Rod Materials of phantom *Gammex 467*

RMI 467 Gammex	**Physical density, g/cm^3**	**Electron density relative to water**	**HU_Theoretical**	**HU_Measured**	**diff. %**
LN-300 Lung	0.290	0.286	-683	-619	-9.4
LN-450 Lung	0.480	0.463	-565	-464	-17.9
BR-12 Breast	0.984	0.961	-46	-57	23.1
AP6 Adipose	0.944	0.927	-105	-104	-0.7
BRN-SR2 Brain	1.052	1.048	15	18	23.3
CT Solid Water1	1.015	0.986	6	5	-27.4
LV1 Liver	1.093	1.061	87	100	14.8
B200 Bone Mineral	1.142	1.095	309	157	-49.2
IB Inner Bone	1.134	1.087	284	163	-42.5
CB2-30% CaCO3	1.332	1.277	575	292	-49.2
CB2-50% CaCO3	1.559	1.469	1057	651	-38.4
SB3 Cortical Bone	1.810	1.683	1602	845	-47.3

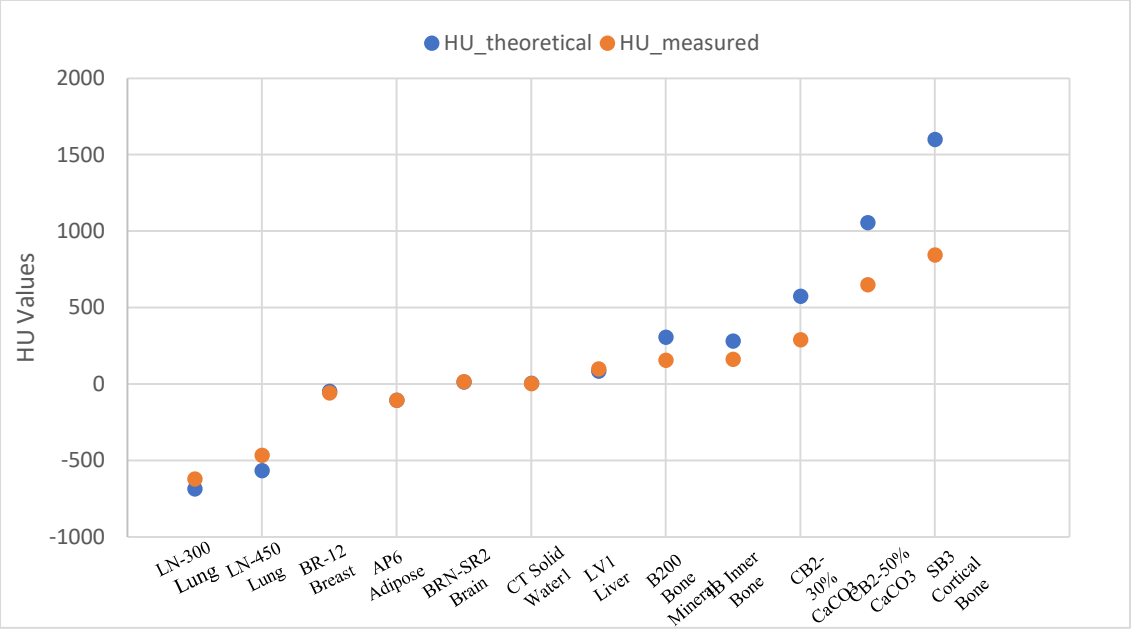

Fig. 33. CT calibration curves measured with *Gammex 467* phantom

Fig. 34 is the calibration curve for the range of different materials of commercial phantom *Gammex 467* and describes the relationship between the electron density relative to water and HU for these different materials.

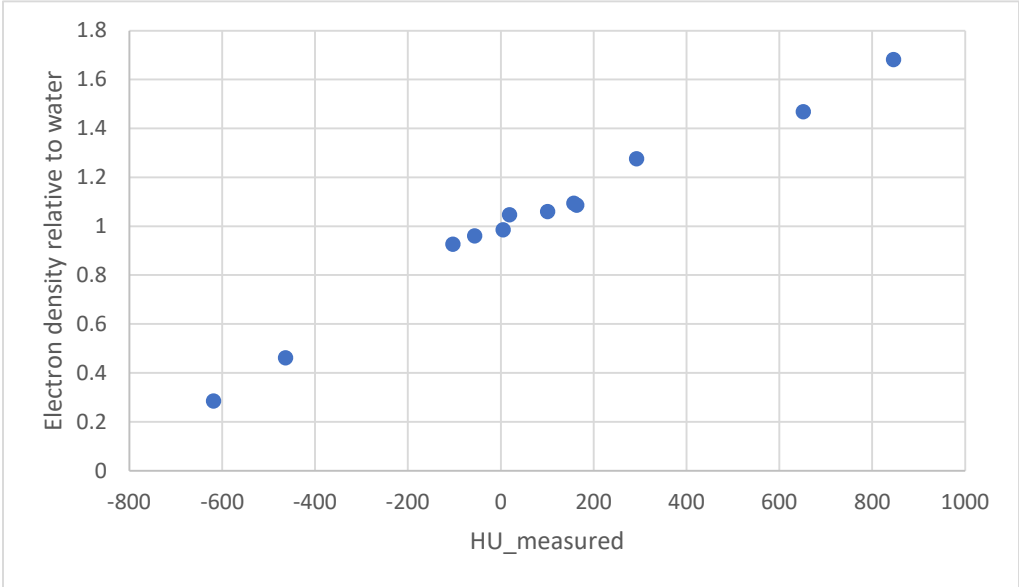

Fig. 34. The relationship between Hounsfield Units (HU) and relative electron density for materials

It can be believed that the small variations for HU values between the two phantoms can be attributed to manufacturing tolerances on material properties and statistical variations between repeated scans.

3.2. HU uniformity measurement

Results related to the uniformity are shown in Table 6. These results show, that the values of HU that have been measured in the center of a uniform slice and the four peripheries' ROIs. The stability of HU values from the ROI_{center} to the $ROI_{periphery}$ of the image slice of a uniform density material is an indication of image uniformity. It can be mentioned that, if there is a significant variation of HU values in both regions (ROI_{center}, $ROI_{periphery}$), the image is nonuniform. The difference in the mean HU between a peripheral and a central region of a homogeneous slice was < 8HU which is in good agreement with study results presented by M. Maqbool [62]. The uniformity index has been measured by the maximum difference between all HU average values of the different ROIs in absolute HU values as shown in Table 6.

Table 6. HU uniformity values of different ROIs during performed monthly

HU uniformity (April)	**HU**	**diff, %**
ROI periphery 1	188	0.0
ROI periphery 2	186	1.0
ROI periphery 3	189	0.5
ROI periphery 4	191	2.0
ROI (center)	185	2.0
The average value of HU of all ROIs	188	
HU uniformity (May)	**HU**	**diff, %**
ROI periphery 1	183	1.0
ROI periphery 2	185	0.0
ROI periphery 3	190	2.0
ROI periphery 4	188	2.0
ROI periphery (center)	182	2.0
The average value of HU of all ROIs	185	

The error of the difference in ROI periphery 1, ROI periphery 2, ROI periphery 3. ROI periphery 4, and ROI periphery centre were 0%, 10%, 0.5%, 2%, and 2%, respectively for April test and were 1%, 0%, 2%, 2% respectively for May test are presented in Fig.35. It was observed that the deviation from baseline values does not exceed ± 10 HU.

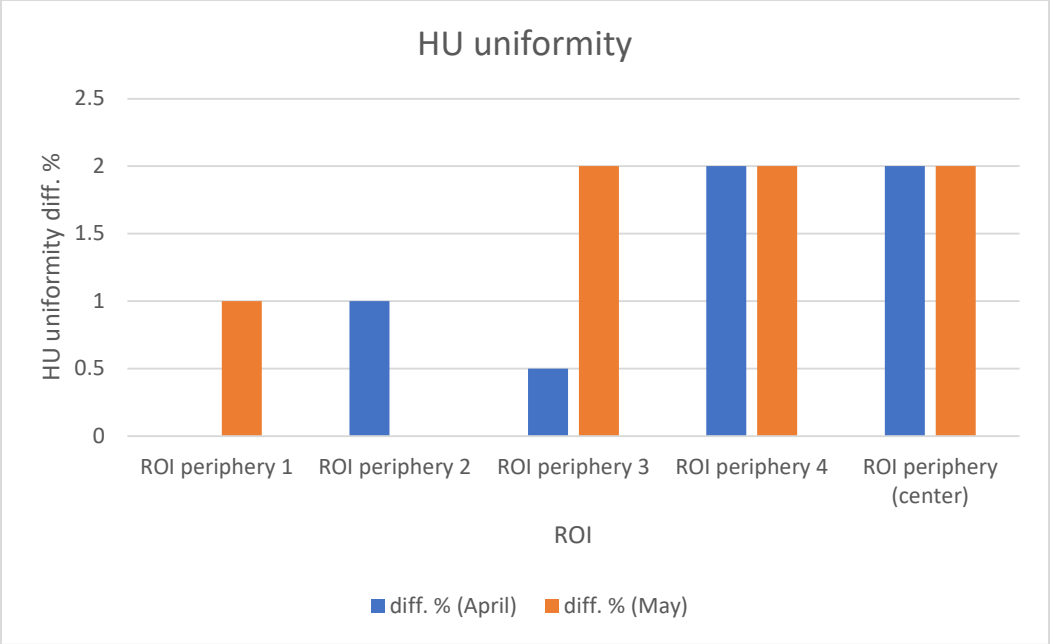

Fig. 35. HU uniformity of different ROIs during performed monthly

A study, which was performed by Stock M et al. [41] where the uniformity index (UI) of different CBCT protocols (low-quality, medium-quality protocol, medium-quality with using a filter (bow-tie filter), high-quality, and high-quality with using the filter) used for quality assurance were evaluated. .The values of UI for each protocol were −0.36, −4.46, −6.0, −0.63, 0.62% respectively. A negative impact on the uniformity was observed for medium-quality protocol when the bow-tie filter was applied (−6.0%), while this trend has not been observed when the filter was applied in the high-quality protocol. The worst values were observed for protocols that use medium-quality and medium-quality with using the filter because of ring artifacts.

Another study was done by Garayoa J [75] where the uniformity index (UI) of CBCT image was 21±3 HU, which indicates the presence of cupping effect. The cupping effect of CBCT images means that the central part of the image is denser than the periphery parts.

Garayoa J also studied the appearance of the artifact when the half-fan filter is used. Garayoa J discussed the uniformity of the image that was obtained with the CBCT in the full-fan mode and a reduction in the SNR value was observed due to the bowtie wobble artifact which has a relevant relationship with the filter motion with gantry rotation.

Therefore, due to these studies, could be concluded, that the uniformity of CBCT images is influenced by the artifacts resulting from scattering and beam hardening.

3.3. Noise, SNR, and CNR measurement

The distribution of HU values for the ROI of the homogenous slice is shown in figure 36. The Image noise is given by the standard deviation of the HU values.

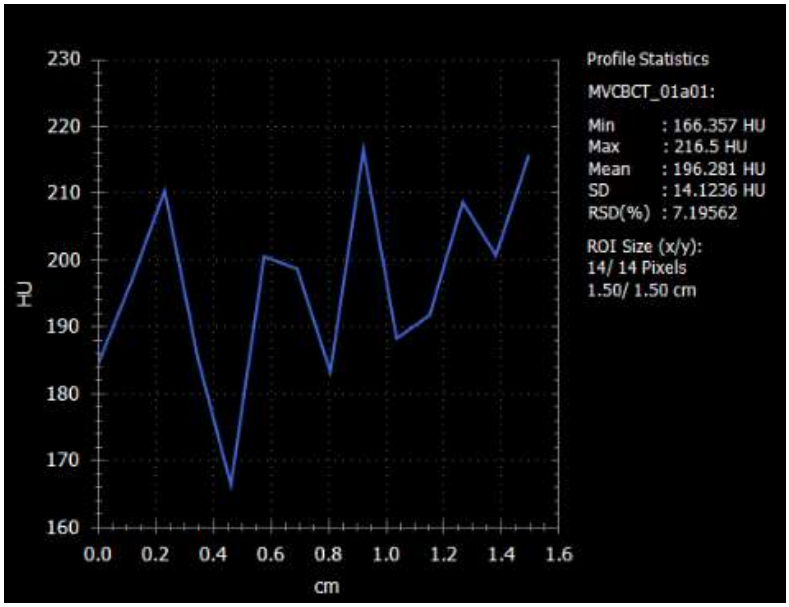

Fig. 36. Profile statistics of the noise measurement

Table 7 shows the analysis of the Single-to-Noise Ratio (SNR) of the selected slices where values were equal to 3.4 for the April test and 2.9 for the May test by calculating the average standard deviation ratio (RSD) of the selected slices. The large value of SNR is an indication of less viewed noise in the image.

Table 7. Signal-to-Noise Ratio (SNR) measurement

Slice No.	1	2	3	4	5	SNR
RSD* % (April)	3.77	3.62	2.96	3.14	3.54	3.4
RSD* % (May)	3.46	2.88	3.48	2.65	2.2	2.9

Table 8 shows the analysis of the Contrast-to-Noise Ratio (CNR) of the selected slices where values were 13.26 for the April test and 8.5 for the May test which have been calculated by using Eq. 5. The large value of CNR is an indication of less noise. A similar tendency of CNR results was observed in some other studies.

A study was performed by Stock M et al. [41] where the CNR was evaluated for CBCT Linc. The CNR (CNR = 13.9) is in good agreement with our study result which is (CNR = 13.3).

In Garayoa J study [75], they studied the influence of the reconstruction filter on the CBCT images where the use of the sharp filter led to an increase in the noise, and therefore the SNR decreases, while by using the smooth filter the SNR was enhanced by reducing the noise.

Table 8. Contrast-to-Noise Ratio (CNR) measurement

Materials (April)	HU	SD	RSD	CNR
Polystyrene	21.52	11.41	52.99	13.26
PMMA_theor	155	11.13	6.58	
Measured	169.19			
Materials (May)	**HU**	**SD**	**RSD**	**CNR**
Polystyrene	28.43	7.5	21.04	8.5
PMMA_theor	155	12.5	7.1	
Measured	151.7			

3.4. Low contrast variability measurement

Table 9 demonstrated the values of low contrast variability which have been calculated using Eq.6. The low contrast visibility is directly proportional to the image noise. The lower value of LCV indicates the good differentiation between regions with small differences in density and less presence of noise in the image and better visualization of soft tissue.

Table 9. Low contrast variability (LCV) measurement

Materials	HU	SD	LCV %
Polystyrene	20.81	7.93	0.29
PMMA_theor	155	6.3	

A study was performed by Stock M et al. [74] the variation of LCV values depended on the parameters in the imaging protocols for the linac CBCT. For example, decreasing mA or kV settings led to increasing the value of LCV as well as decreasing in uniformity index.

Another study was done by Garayoa J [75] where the low-contrast sensitivity was affected by the reconstruction filter used in the CBCT.

3.5. Slice Thickness measurement

It is recommended to evaluate the profiles on both air-gap structures and average the result to improve the accuracy of the measured slice thickness value. Fig. 37 has been represented the horizontal profiles of the two ROIs which contain the air gap1 and air gap 2 to measure the slice thickness. Fig. 38 has represented the profile statistics.

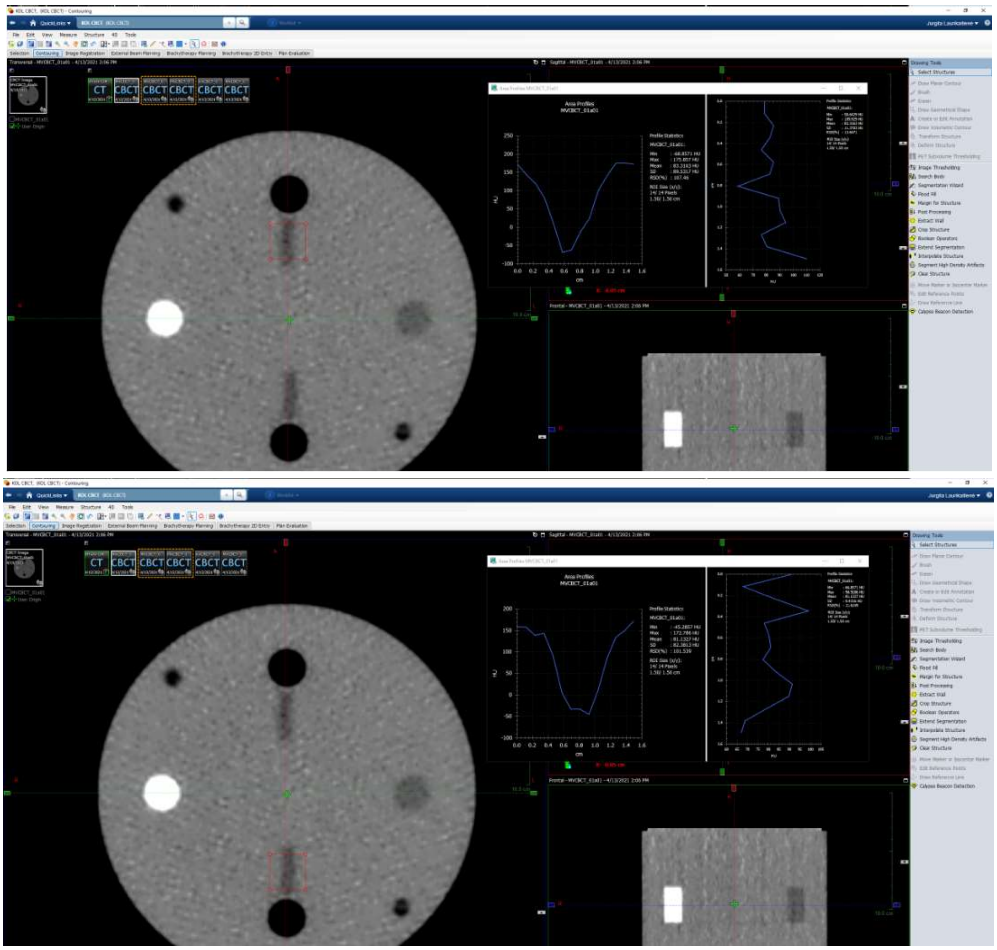

Fig. 37. Central slice of CBCT reconstruction of slice thickness measurement and profile statistics (profile1 and profile2)

The horizontal profiles have been shifted to be centered at position 0 mm (Fig. 38).

A study was done by Garayoa J [75] where the measured slice width using the ramp method over the CBCT images for the standard reconstruction filter was 2.2 ± 0.1 mm.

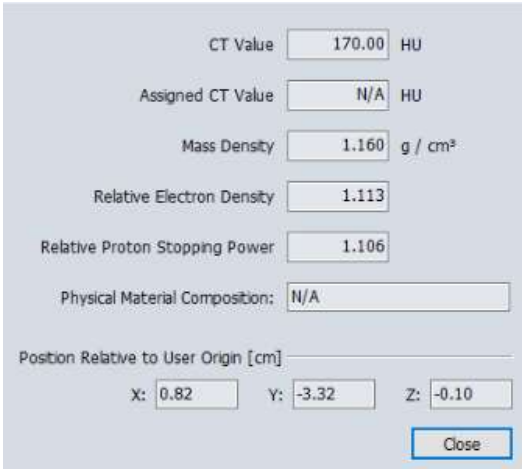

Fig. 38. Measurement of physical properties of slice thickness

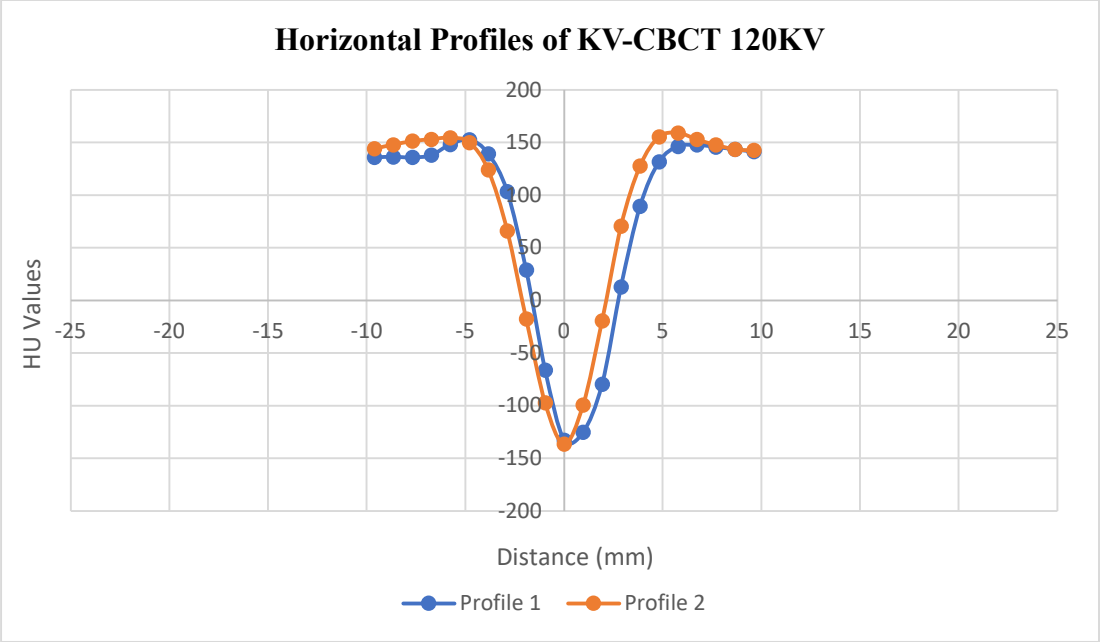

Fig. 39. Horizontal Profiles of KV-CBCT image

The dots represent pixel positions. The baseline is close to the nominal value of 120 HU for PMMA material, with a minimum at -132 HU and -136 HU, the FWHM value is evaluated as 3.33 and 4.19 for the April test and 3.4 and 3.7 for the May test, which leads to an average FWHM value of 3.76 mm and 3.55 for the April and May test respectively, corresponding to a slice thickness of 2.16 mm for April test and 2.04 mm for May test as shown in Table 10.

The average slice thickness (Thickness = 2.16 and 2.04 mm) is in good agreement with the value that was recommended by the manufacturer of phantom *QUART* (Default value = 2.00 mm).

Table 10. Slice Thickness measurement

Slice Thickness measurement	Profile 1	Profile 2	Average
FWHM, mm (April)	3.33	4.19	3.76
Slice thickness, mm (April)	1.92	2.41	2.17
FWHM, mm (May)	3.4	3.7	3.55
Slice thickness, mm (May)	1.96	2.13	2.05

Slice thickness has been evaluated by measuring FWHM. Figure 41 has been shown the value of the width structure, which was equal to 3.6 mm. Applying eq.8, the slice thickness was calculated as 2.07 mm, which is in good agreement with the value that was recommended by the manufacturer of phantom *QUART* (Default value = 2.00 mm).

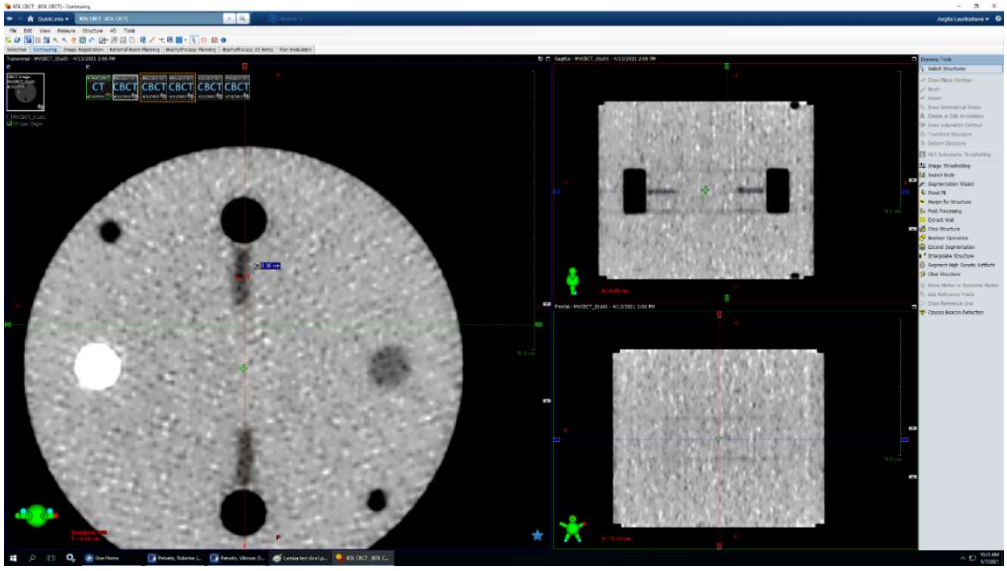

Fig. 39. Central slice of CBCT reconstruction of visual slice thickness measurement

3.6. Geometric scaling measurement

The geometric scaling has been verified by measuring the diameter both in horizontal and vertical direction (Fig. 40).

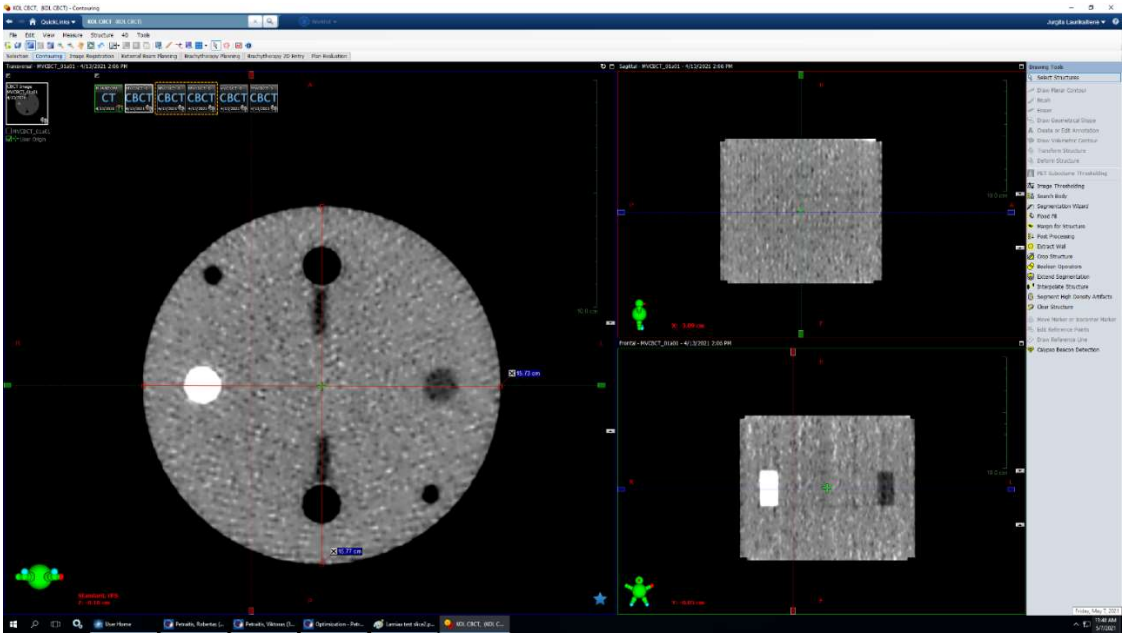

Fig. 40. Central slice of CBCT reconstruction of visual slice thickness measurement geometric scaling measurement (Vertical).

Table 11 shows the Geometric scaling measurement. The diameter of the phantom was 15.73 cm and 15.77 cm vertically and horizontally respectively. The accuracy of scaling measurement was 0.0025%. the accuracy of measurement is in agreement with the value that was recommended by the manufacturer which is < 1%.

Table 11. Geometric scaling measurement

Scaling	Horizontal Diameter (cm)	Vertical Diameter (cm)	Diff. %	Accuracy
(April)	15.73	15.77	0.25	< 1%
(May)	15.85	15.79	0.37	< 1%

3.7. Suggested Protocol

Due to the quality control tests were prepared measurement protocols and offered to use in a clinical practice (Appendix 1.)

Baselines and tolerances have been set for each image quality parameter based on the previous data (Table 12). This protocol will be used to identify an appropriate way to set applicable baselines and tolerances that would account for the variability of the measurements while also being able to identify significant changes in the image quality.

Table 12. Routine kV-CBCT QC test items and tolerance are suggested to be used for *Halcyon*.

CBCT image quality Test	Frequency	Tolerance
Accuracy	Monthly	Baseline
Uniformity	Monthly	2%
Noise	Monthly	2%
Low contrast resolution	Monthly	2%
Geometrical accuracy	Monthly	<1%

Conclusions

1. There are a variety of commercial IGRT technologies available to apply, the main advantages and disadvantages of different modalities of image-guided radiotherapy have been analyzed. Depending on the used clinical scenarios the IGRT system can be chosen. Even the image-guidance process means an additional time and exposure dose to each radiation therapy session, but this dose is beneficial and ensures the quality of the treatment.

2. Image quality control tests of kV CBCT have been performed to ensure the accuracy of visualization and localization of tumors. The assessments and analysis of the results have been performed monthly (April and May tests) by using commercially available phantom (*QUART*), treatment planning system (*Eclipse*), and software tools of (*ImageJ* and *RadiAnt*). The results showed, that correspondence HU values were measured experimentally with known theoretical values. HU values of the center and periphery ROIs of the slice differed in a range from 189.0 – 191.1 HU and 182.0-190.0 for $ROI_{periphery}$ and was 185.0 and 182.0 for ROI_{center} for April and May tests, which is an indication of image uniformity. The values of SNR and CNR were 3.4, 2.9, and 13.3, 8.5 for the April and May results, respectively. The larger value of SNR is an indication of less viewed noise in the image, while the large value of CNR is an indication of less noise. The lower value of LCV (0.29%) indicated the good differentiation between regions with small differences in density and less presence of noise in the image and better visualization of soft tissues. The average slice thickness was evaluated experimentally in Aprile and May and determined as 2.16 mm 2.04, and 2.07 mm, respectively. Slice thickness measurements were in good agreement with the value that is recommended by the manufacturer of phantom *QUART* (Default value = 2.00 mm). The geometric scaling has been verified by measuring the diameter both in the horizontal and vertical direction and the accuracy of measurement was < 1% as is recommended.

3. According to image quality assurance, that has been done, was prepared a protocol for quality control, which will be used in clinical practice.

List of references

1. American College of Radiology. ACR-AAPM Technical Standard for medical physics performance monitoring of image-guided radiation therapy (IGRT). 2014.
2. Filipa Guerreiro, Enrica Seravalli, Geert O. Janssens, Cees P. van de Ven, Marry M. van den Heuvel-Eibrink & Bas W. Raaymakers (2018) Intra- and inter-fraction uncertainties during IGRT for Wilms' tumor, Acta Oncologica, 57:7, 941-949, DOI: 10.1080/0284186X.2018.1438655.
3. Gupta T, Narayan CA. Image-guided radiation therapy: Physician's perspectives. J Med Phys. 2012;37(4):174-182. doi:10.4103/0971-6203.103602.
4. Goyal S, Kataria T. Image guidance in radiation therapy: techniques and applications. Radiol Res Pract. 2014;2014:705604.
5. Barker JL, Garden AS, Ang KK, O'Daniel JC, Wang H, Court LE, et al. Quantification of volumetric and geometric changes occurring during fractionated radiotherapy for head-and-neck cancer using an integrated CT/linear accelerator system. Int J Radiat Oncol Biol Phys 2004;59:960–70.
6. Sonke JJ, Aznar M, Rasch C. Adaptive Radiotherapy for Anatomical Changes. Semin Radiat Oncol 2019;29:245–57.
7. Wortel RC, Incrocci L, Pos FJ, Lebesque JV, Witte MG, van der Heide UA, van Herk M, Heemsbergen WD. Acute toxicity after image-guided intensity modulated radiation therapy compared to 3D conformal radiation therapy in prostate cancer patients. Int J Radiat Oncol Biol Phys. 2015 Mar 15;91(4):737-44.
8. American College of Radiology. ACR practice parameter for intensity modulated radiation therapy (IMRT). 2016.
9. American College of Radiology. ACR–ASTRO practice parameter for the performance of stereotactic body radiation therapy. 2014.
10. Tiong A, Lao L, MacKean J, Goonetilleke M, Kron T. Faculty of Radiation Oncology Position Paper on the use of Image-Guided Radiation Therapy. J Med Imaging Radiat Oncol. 2016 Dec;60(6):772-780.
11. Bujold A, Craig T, Jaffray D, Dawson LA. Image-guided radiotherapy: has it influenced patient outcomes? Semin Radiat Oncol 2012; 22: 50–61
12. Schwarz, M., Giske, K., Stoll, A. et al. IGRT versus non-IGRT for postoperative head-and-neck IMRT patients: dosimetric consequences arising from a PTV margin reduction. Radiat Oncol 7, (2012) 133.
13. Pushpa N CH, Umesh M. Clinical Challenges in Image Guided Radiation Therapy (Igrt) For Gynaecological Malignancies. Curr Trends Clin Med Imaging. 2019; 2(5): 555608. DOI: 10.19080/CTCMI.2019.02.555608
14. Zelefsky MJ, Kollmeier M, Cox B, Fidaleo A, Sperling D, Pei X, Carver B, Coleman J, Lovelock M, Hunt M. Improved clinical outcomes with high-dose image guided radiotherapy compared with non-IGRT for the treatment of clinically localized prostate cancer. Int J Radiat Oncol Biol Phys. 84(1) 2012: 125-129.
15. Nguyen, Nam Phong, et al. "Image-guided radiotherapy for locally advanced head and neck cancer". Front. Oncol. 3, 2013:172. doi: 10.3389/fonc.2013.00172.

16. Kupelian PA, Willoughby TR, Reddy CA, Klein EA, Mahadevan A. Impact of image guidance on outcomes after external beam radiotherapy for localized prostate cancer. Int J Radiat Oncol Biol Phys; 70,2008: 1146–50.
17. INTERNATIONAL ATOMIC ENERGY AGENCY, Radiation Protection and Safety of Radiation Sources: International Basic Safety Standards, IAEA Safety Standards Series No. GSR Part 3, IAEA, Vienna (2014).
18. INTERNATIONAL ATOMIC ENERGY AGENCY, Introduction of Image Guided Radiotherapy into Clinical Practice, Human Health Reports No. 16, IAEA, Vienna (2019).
19. Zhou, L., Bai, S., Zhang, Y. et al. Imaging Dose, Cancer Risk and Cost Analysis in Image-guided Radiotherapy of Cancers. Sci Rep 8, (2018) 10076. https://doi.org/10.1038/s41598-018-28431-9.
20. Kataria T., Abhishek A., Chadha P., Nandigam J. Set-up uncertainties: online correction with X-ray volume imaging. Journal of Cancer Research and Therapeutics. 2011;7(1):40–46.doi: 10.4103/0973-1482.80457.
21. Kataria T., Gupta D., Karrthick K., et al. Frame-based radiosurgery: is it relevant in the era of IGRT? *Neurology India*. 2013;61(3):277–281. doi: 10.4103/0028-3886.115068.
22. Division of Radiation Oncology, Medanta Cancer Institute, Medanta-The Medicity, Gurgaon, Haryana 122001, India
23. Chen, G.T.Y., Sharp, G.C. & Mori, S. A review of image-guided radiotherapy. Radiol Phys Technol 2, 1–12 (2009). https://doi.org/10.1007/s12194-008-0045-y
24. Sun B, Chang J, Rong Y. The more IGRT systems, the merrier?. J Appl Clin Med Phys. 2017;18(4):7-11. doi:10.1002/acm2.12126.
25. Richter A, Polat B, Lawrenz I, et al. Initial results for patient setup verification using transperineal ultrasound and cone beam CT in external beam radiation therapy of prostate cancer. Radiat Oncol. 2016;11:147.
26. Goyal S, Kataria T (2014) Image-Guided Radiation Therapy. J Nucl Med Radiat Ther 5: 179.
27. Wong J.W. (2013) Electronic Portal Imaging Devices (EPID). In: Brady L.W., Yaeger T.E. (eds) Encyclopedia of Radiation Oncology. Springer, Berlin, Heidelberg
28. Korreman S, Rasch C, McNair H, et al. The European Society of Therapeutic Radiology and Oncology-European Institute of Radiotherapy (ESTRO-EIR) report on 3D CT-based in-room image guidance systems: a practical and technical review and guide. Radiother Oncol 2010;94:129-144.
29. Qi X.S. (2017) Image-Guided Radiation Therapy. In: Maqbool M. (eds) An Introduction to Medical Physics. Biological and Medical Physics, Biomedical Engineering. Springer, Cham.
30. Xiao Y. (2013) Image-Guided Radiation Therapy (IGRT): kV Imaging. In: Brady L.W., Yaeger T.E. (eds) Encyclopedia of Radiation Oncology.
31. Held M, Cremers F, Sneed PK, Braunstein S, Fogh SE, Nakamura J, Barani I, Perez-Andujar A, Pouliot J, Morin O. Assessment of image quality and dose calculation accuracy on kV CBCT, MV CBCT, and MV CT images for urgent palliative radiotherapy treatments. J Appl Clin Med Phys. 2016 Mar 8;17(2):279-290. doi: 10.1120/jacmp.v17i2.6040. PMID: 27074487; PMCID: PMC5874969
32. Holmes T. (2013) Image-Guided Radiation Therapy (IGRT): TomoTherapy. In: Brady L.W., Yaeger T.E. (eds) Encyclopedia of Radiation Oncology. Springer, Berlin, Heidelberg.

33. Van Gestel D, Verellen D, Van De Voorde L, de Ost B, De Kerf G, Vanderveken O, Van Laer C, Van den Weyngaert D, Vermorken JB, Gregoire V. The potential of helical tomotherapy in the treatment of head and neck cancer. Oncologist. 2013 Jun;18(6):697-706.
34. Stankovic U, Ploeger LS, van Herk M & Sonke JJ (2017) Optimal combination of anti-scatter grids and software correction for CBCT imaging. Med Phys 44, 4437–4451]
35. Jarema T & Aland T (2019) Using the iterative kV CBCT reconstruction on the Varian Halcyon linear accelerator for radiation therapy planning for pelvis patients. Phys Med 68, 112–116.
36. Bryce-Atkinson A, Marchant T, Rodgers J, Budgell G, McWilliam A, Faivre-Finn C, Whitfield G & van Herk M (2019) Quantitative evaluation of 4D Cone beam CT scans with reduced scan time in lung cancer patients. Radiother Oncol 136, 64–70.
37. Venkatesh E, Elluru SV. Cone beam computed tomography: basics and applications in dentistry. J Istanb Univ Fac Dent.;51.3(Suppl1)2017:S102-S121. Published 2017 Dec 2. doi:10.17096/jiufd.00289.
38. Srinivasan K, Mohammadi M, Shepherd J. Applications of linac-mounted kilovoltage Cone-beam Computed Tomography in modern radiation therapy: A review. Pol J Radiol. 2014;79:181-193. Published 2014 Jul 3. doi:10.12659/PJR.890745.
39. Silva Maurício Barbosa Guerra da, Sant'Anna Eduardo Franzotti. The evolution of cephalometric diagnosis in Orthodontics. Dental Press J. Orthod. [Internet]. 2013 June [cited 2021 May 17] ; 18(3): 63-71.
40. Schulze R, Heil U, Gross D, Bruellmann DD, Dranischnikow E, Schwanecke U, Schoemer E. Artefacts in CBCT: a review. Dentomaxillofac Radiol. 2011 Jul;40(5):265-73. doi: 10.1259/dmfr/30642039.
41. Stock M, Pasler M, Birkfellner W, Homolka P, Poetter R, Georg D. Image quality and stability of image-guided radiotherapy (IGRT) devices: A comparative study. Radiother Oncol. 2009 Oct; 93(1):1-7.
42. Lechuga L, Weidlich GA. Cone Beam CT vs. Fan Beam CT: A Comparison of Image Quality and Dose Delivered Between Two Differing CT Imaging Modalities. Cureus. 2016;8(9):e778. Published 2016 Sep 12. doi:10.7759/cureus.778.
43. Djordjević, M.. “Evaluation of Geometric Accuracy and Image Quality of an On-Board Imager (OBI).” (2007).
44. Batte, Catherine Leigh, "Accuracy of SRS dose delivery using the TomoTherapy Hi-Art System" (2010). LSU Master's Theses. 1272.
45. Massaccesi M. (2020) CT in Room Gating During Radiotherapy. In: Beets-Tan R., Oyen W., Valentini V. (eds) Imaging and Interventional Radiology for Radiation Oncology. Medical Radiology. Springer, Cham
46. www.siemens.com/medical
47. Yoo S, Kim GY, Hammoud R, Elder E, Pawlicki T, Guan H, Fox T, Luxton G, Yin FF, Munro P. A quality assurance program for the on-board imagers. Med Phys. 33(11) 2006:4431-47.

48. Morrow NV, Lawton CA, Qi XS, Li XA. Impact of computed tomography image quality on image-guided radiation therapy based on soft tissue registration. Int J Radiat Oncol Biol Phys. 2012 Apr 1;82(5):e733-8.
49. Chan M, Yang J, Song Y, Burman C, Chan P, Li S. Evaluation of imaging performance of major image guidance systems. Biomed Imaging Interv J. 2011 Apr;7(2):e11.].
50. Grégoire V, Guckenberger M, Haustermans K, et al. Image guidance in radiation therapy for better cure of cancer. Mol Oncol. 2020;14(7):1470-1491. doi:10.1002/1878-0261.12751
51. Dang A, Kupelian PA, Cao M, Agazaryan N, Kishan AU. Image-guided radiotherapy for prostate cancer. Transl Androl Urol. 2018;7(3):308-320. doi:10.21037/tau.2017.12.37.
52. Western C, Hristov D, Schlosser J. Ultrasound Imaging in Radiation Therapy: From Interfractional to Intrafractional Guidance. Cureus. 2015;7(6):e280. Published 2015 Jun 20.
53. Sen HT, Bell MAL, Zhang Y, et al. System Integration and In Vivo Testing of a Robot for Ultrasound Guidance and Monitoring During Radiotherapy. IEEE Trans Biomed Eng. 2017;64(7):1608-1618. doi:10.1109/TBME.2016.2612229.
54. Stenmark MH, Hamstra DA. Image-Guided Strategies for Prostate Cancer. In: Thomas CR, editor. Radiation Medicine Rounds Prostate Cancer. Demos Medical Publishing, 2011:113-30.
55. Hachadorian, R.L., Bruza, P., Jermyn, M. et al. Imaging radiation dose in breast radiotherapy by X-ray CT calibration of Cherenkov light. Nat Commun 11, 2298 (2020).
56. Arivarasan I, Anuradha C, Subramanian S, et al. Magnetic resonance image guidance in external beam radiation therapy planning and delivery. Jpn J Radiol 2017;35:417-26.
57. https://viewray.com/
58. Bissonnette, Jean-Pierre, et al. "Quality assurance for image-guided radiation therapy utilizing CT-based technologies: a report of the AAPM TG-179." Medical physics 39.4 (2012): 1946-1963.
59. Bushberg, Jerrold T., and John M. Boone. The essential physics of medical imaging. Lippincott Williams & Wilkins, 2011
60. Anne TK et al (2010) Evaluation of subjective assessment of the low-contrast visibility in constancy control of computed tomography. Radiat Prot Dosim 139(1–3):449–454
61. de Las Heras Gala, Hugo, et al. "Quality control in cone-beam computed tomography (CBCT) EFOMP-ESTRO-IAEA protocol (summary report)." Physica Medica 39 (2017): 67-72.
62. M. Maqbool (ed.), An Introduction to Medical Physics, Biological and Medical Physics, Biomedical Engineering, AG 2017, corrected publication 2018, DOI 10.1007/978-3-319-61540-0_1.
63. Boda-Heggemann J, Lohr F, Wenz F, Flentje M, Guckenberger M. kV cone-beam CT-based IGRT: a clinical review. Strahlenther Onkol. 2011;187(5):284–91. doi:10.1007/s00066-011-2236-4
64. Yan H, Cervino L, Jia X, Jiang SB. A comprehensive study on the relationship between the image quality and imaging dose in low-dose cone beam CT. Phys Med Biol. 2012;57(7):2063-2080. doi:10.1088/0031-9155/57/7/2063.
65. Nakahara, Satomi, Masayuki Tachibana, and Yoichi Watanabe. "One-year analysis of Elekta CBCT image quality using NPS and MTF." Journal of applied clinical medical physics 17.3 (2016): 211-222.

66. S. Panda, J. Swamidas, S. Chopra, A. Mangaj, A. Fogliata, P. Kupelian, J. P. Agarwal, L. Cozzi, Treatment planning comparison of volumetric modulated arc therapy employing a dual-layer stacked multi-leaf collimator and helical tomotherapy for cervix uteri, Radiation Oncology, 10.1186/s13014-020-1473-z, 15, 1, (2020).
67. Li Y, Netherton T, Nitsch PL, Balter PA, Gao S, Klopp AH, Court LE. Normal tissue doses from MV image-guided radiation therapy (IGRT) using orthogonal MV and MV-CBCT. J Appl Clin Med Phys. 2018 May;19(3):52-57.
68. https://www.varian.com/products/radiotherapy/treatment-delivery/halcyon.
69. Cai B, Laugeman E, Mazur TR, Park JC, Henke LE, Kim H et al. Characterization of a prototype rapid kilovoltage x-ray image guidance system designed for a ring shape radiation therapy unit. Medical physics. 2019 Mar;46(3):1355-1370.
70. www.quart.de
71. http://rsb.info.nih.gov/ij
72. Elstrøm, Ulrik V., et al. "Evaluation of image quality for different kV cone-beam CT acquisition and reconstruction methods in the head and neck region." Acta Oncologica 50.6 (2011): 908-917.
73. Chan MF, Yang J, Song Y, Burman C, Chan P, Li S. Evaluation of imaging performance of major image guidance systems. Biomed Imaging Interv J. 2011;7(2):e11.
74. Stock M, Pasler M, Birkfellner W, Homolka P, Poetter R, Georg D. Image quality and stability of image-guided radiotherapy (IGRT) devices: A comparative study. RadiothOncol 2009;93(1):1-7.
75. Garayoa J, Castro P. A study on image quality provided by a kilovoltage cone-beam computed tomography. J Appl Clin Med Phys. 2013 Jan 7;14(1):3888.

Appendices

Appendix 1. Worksheet for Image Quality Assurance Protocol

Quality Control Protocol

Worksheet for Image Quality Assurance

User: **Date:**

System Info.:

Linc System:		
Phantom:		
Phantom diameter:		
Selected Protocol	kV CBCT	
Scanning Parameters		
Analysis Software		

HU Accuracy measurement

ROIs	Nominal HU value	Measured HU average	diff. %	Tolerance
				Baseline

HU uniformity measurement

ROIs	Nominal HU value	diff. %	Tolerance
ROI periphery 1			2%
ROI periphery 2			
ROI periphery 3			
ROI periphery 4			
ROI center			
verage value of HU of all ROIs			

Signal-to-Noise Ratio (SNR) measurement

slice No.	SNR - RSD%
1	
2	
3	
4	
5	
Average (SNR)	

Contrast-to-Noise Ratio (CNR) measurement

$$CNR = \frac{[abs\,(HU\ insert - HU\ background)]}{\sqrt{\sigma 2\ insert + \sigma 2\ background}}$$

Material	HU	SD
Insert		
background		
CNR		

Low contrast variability measurement

$$LCV = \frac{2.75(\sigma 1 + \sigma 2)}{P1 - P2}$$

Material	HU	SD	Tolerance
Polystyrene			2mm
PMMA			
LCV			

Slice Thickness measurement

$$S = 0.577 * FWHM$$

Slice Thickness measurement	Profile 1	Profile 2	Average	Tolerance
FWHM, mm				2%
Slice thickness, mm				

Geometric scaling measurement

Horizontal Diameter (cm)	Vertical Diameter (cm)	Diff. %	Accuracy	Tolerance
				<1